DOI

Elsevier Editorial System(tm) for
Atmospheric Research

Manuscript Draft

Manuscript Number: ATMOSRES-D-16-00491R1

Title: Origin and pathways of the mineral dust transport to two Spanish EARLINET sites: effect on the observed columnar and range-resolved dust optical properties

Article Type: Research Paper

Section/Category: aerosol particles

Keywords: Saharan dust events, Barcelona and Granada EARLINET sites, aerosol optical properties, dust plume geometrical structure, backward trajectories

Corresponding Author: Dr. Florian A Mandija, PhD

Corresponding Author's Institution: Dept. of Physics, Fac. Nat. Sci., Univ. of Shkodra, Shkoder, Albania; Andalusian Institute for Earth System Research (IISTA-CEAMA), Granada, Spain

First Author: Florian A Mandija

Order of Authors: Florian A Mandija; Michaël Sicard; Adolfo Comerón; Lucas Alados-Arboledas; Juan Luis Guerrero Rascado; Ruben Barragan; Juan Antonio Bravo-Aranda; Maria Jose Granados-Muñoz; Hassan Lyamani; Constantino Muñoz Porcar; Francisco Rocadenbosch; Alejandro Rodríguez; Antonio Valenzuela; David García Vizcaíno

Abstract: In this paper, is presented a method for estimation of the effect of the transport process to aerosol optical properties. Aerosol optical data retrieved by lidars and sun-photometer measurements, are applied to Saharan dust events observed simultaneously at the two EARLINET/AERONET sites of Barcelona and Granada during the periods of June-September of 2012 and 2013. For this purpose, elastic lidar profiles and sun-photometer columnar retrievals are analyzed together with satellite observations and dust forecast models. Granada presents more than twice Saharan dust outbreaks compared to Barcelona. The scenarios favoring the Saharan dust outbreaks are identified in both places. The mineral dust originating in the Sahara region and arriving at both stations is usually transport wither over the Atlas Mountains or through an Atlantic pathway. Analyses of dust events affecting both stations reveal how differences in the transport process lead to differences in the aerosol optical properties measured at each station. Mean dust-related Ångström exponent is 1.8 times higher in Barcelona than in Granada. This difference is a result of the additional contribution of anthropogenic aerosol, mainly in the aerosol fine mode, during the transport of the mineral dust plume over the Iberian Peninsula.

Highlights

- Coincidence Saharan dust events over the Granada and Barcelona stations are studied.
- Column integrated and the vertical resolved from AERONET and EARLINET are used.
- Cluster analysis of Hysplit trajectories was involved in this study.
- Key scenarios of Saharan dust intrusions over Iberian Peninsula are identified.
- Variations of the optical properties, during the transport process are determined.

Origin and pathways of the mineral dust transport to two Spanish EARLINET sites: effect on the observed columnar and range-resolved dust optical properties

1. Introduction

Mineral dust is one of the most important components of the atmospheric aerosol loading. Mineral dust constitutes about 75% of the global aerosol mass load and 25% of the global aerosol optical depth (Kinne et al., 2006). Dust is one of the principal aerosol types in the atmosphere and plays an important role in climate change via a number of complex processes. Dust aerosols impact the radiation budget of the Earth–atmosphere system, both directly by scattering and absorbing solar and terrestrial thermal radiation, and also indirectly by modifying cloud optical properties and lifetimes. The shortwave radiative forcing of dust aerosols can be either positive or negative, whilst the longwave radiative forcing is always positive (Tegen et al., 1996; Sokolik et al., 2001; Ramanathan et al., 2007; Perrone and Bergamo, 2011; Piedeherro et al., 2014; Obregon et al., 2015).

North Africa is widely considered as the Earth's largest source of dust (Prospero et al., 2002; Liu et al. 2008; Pey et al., 2013). A large amount of Saharan dust is transported over the Mediterranean, mainly because of cyclone activity in the region (La Fontaine et al., 1990). Aerosols over the Mediterranean originate from different sources, including a marine component, a mineral dust component, mainly due to the proximity to Sahara desert dust and an anthropogenic component (local and long-range pollution) (Barnaba and Gobbi, 2004).

Research on dust intrusions from the Sahara desert and its distribution in the atmosphere has been increasing over the last decade. Aerosol optical properties change rapidly, due to diffusion and aging processes such as coagulation, humidification, scavenging by precipitation and gas to particle phase conversion (Schuster et al., 2006). These processes, combined with varying source strength and/or advection by meteorological processes, create a dynamic atmospheric constituent affecting climate, environment and public health (IPCC, 2013).

Measurements of aerosol properties over the Mediterranean region have been carried out since the 1980s (Smirnov et al., 2002), but most of them were occasional and lasted only for short periods. Other measurements covered longer time periods (Cachorro et al., 2000; Formenti et al., 2001; Sabbah et al., 2001; Tanre et al., 2001; Gerasopoulos et al., 2003; Israelevich et al., 2003; Esposito et al., 2004; Pavese et al., 2009). Analyses based on satellite observations were also performed to identify the transport of Saharan dust (e.g. Moulin et al., 1998; Israelevich et al., 2002; Jamet et al., 2004).

The Saharan dust aerosol properties and their spatial and temporal variability over the Iberian Peninsula during the dust events have already been studied in recent years (Alados-Arboledas et al, 2003, 2008; Lyamani et al., 2005, 2006a, b, 2008; Elias et al., 2006; Mona et al., 2006; Perez

et al., 2006; Dıaz et al., 2007; Guerrero-Rascado et al., 2008, 2009; Cachorro et al., 2008; Sicard et al., 2011; Perez-Ramirez et al., 2012; Valenzuela et al., 2012; Navas-Guzman et a., 2013).

Several parameters can be used for aerosol characterization. The aerosol optical depth AOD is an optical parameter measured by sun-photometers like the ones operating in AERONET (Holben et al., 1998). This parameter represents the extinction of radiation at a certain wavelength that results from the presence of atmospheric aerosols. The Ångström exponent represents the slope of the wavelength dependence of the AOT in logarithmic coordinates:

$$\alpha(\lambda_1, \lambda_2) = -\ln(\tau_{\lambda 2}/\tau_{\lambda 1})/\ln(\lambda_2/\lambda_1)$$

where $\tau_{\lambda 1}$ and $\tau_{\lambda 2}$ represent the aerosol optical depths at the wavelengths λ_1 and λ_2 respectively.

In the solar spectrum, the Ångström exponent AE is a good indicator of the size of the atmospheric particles determining the AOD: $AE_{440\text{-}870}>1$ is mainly determined by fine mode, while $AE_{440\text{-}870}<1$ is largely determined by coarse mode (Kaufman et al., 1994). However, AE alone does not provide unambiguous information on the relative weight of coarse and fine modes on the AOD. Several authors have discussed how the spectral variation of the Ångström exponent can provide further information about the aerosol size distribution (Eck et al., 1999; O'Neill et al., 2001a, b, 2003; Fernández-Gálvez et al., 2013). Kaufman (1993) shows that negative values of the difference $\delta\alpha=AE_{440\text{-}613}-AE_{613\text{-}1003}$ indicate the dominance of fine mode aerosols while positive values of this difference indicate the effect of two separate particle modes.

This study consists of an evaluation of the changes in properties of dust through combined lidar-sunphotometer techniques as it is transported between the cities of Granada and Barcelona. Temporal variation of optical properties, as well as the differences between the patterns of profiles of lidar-mesaured backscatter coefficients at 532 nm (bsc_532 nm) in Granada and Barcelona, gives valuable information about the dust transport between these two EARLINET stations.

The paper has following structure: Instrumentation, tools and methodology are given in Sect.2. Sect.3 presents the characteristics of the dust events over two stations. Later, in Sect.4, we present the scenarios of dust intrusions according to the origins and the pathways. Columnar aerosol properties are discussed in Sect.5. Analysis of the coincidence dust events at both sites is given in Sect.6. Lidar profiling during a case study is presented in Sect.7. At the end, Sect.8 presents the conclusion of this work.

2. Instrumentation, tools, and methodology

2.1 Instrumentation and tools

The Barcelona EARLINET station is located in an urban area of Barcelona in North-East of Spain, (41.389º N, 2.112º E, 115 m altitude asl), quite near the seashore of the western Mediterranean Sea (Pappalardo et al., 2015). The Granada EARLINET station is located in Granada city in the southern part of Spain (37.164º N, 3.60º5 W, 680 m altitude asl). This site is affected directly by Saharan dust intrusions, due to its proximity to the North Africa. Both sites are around 700 km distant from each other. The instrumentation used in this study consists of sun-photometer and lidar systems, located in the stations of Barcelona and Granada. The synergic combination of sun-photometers and lidars enables to improve the knowledge on optical and microphysical properties of aerosols and their vertical distribution (Sicard et al., 2015).

The CIMEL sun–sky photometer CE-318-4 located in Barcelona, part of the Aerosol Robotic Network (AERONET) (Holben et al., 1998), was used to provide the AOD at 675nm and the Ångström exponent, AE at 440-870nm. The estimated accuracy of AOD measurements is about 0.02 at the processing level 2.

Daytime, column-integrated characterization of the atmospheric aerosol in Granada has been also done by using a sun-photometer CE-318-4 included in the AERONET network.

The EARLINET lidar from the Universitat Politecnica de Catalunya in Barcelona was situated at the time of the measurements reported in this paper 600 m away from the sun photometer. The system employs a Nd:YAG laser with second and third harmonic generators emitting three coaxial beams at 355 nm, 532 nm and 1064 nm (fundamental) wavelengths with respective pulse energies of approximately 25 mJ, 55mJ, and 85 mJ, at a repetition rate of 20 Hz. The radiation backscattered by the atmosphere is collected by a 38-cm diameter, 4-m focal length Cassegrain telescope and is guided by an optical fiber bundle to the wavelength separation unit (polychromator), where it is directed to the photodetectors (photomultiplier tubes for the 355-nm and the 532-nm wavelengths, and an avalanche photodiode for the 1064-nm wavelength) converting the optical signal at the corresponding wavelength into an electrical signal being sampled and stored for later analysis. The system has also Raman channels able to measure the radiation of the Raman vibrational-rotational spectrum scattered by atmospheric N_2 at 387 nm (excitation at 355 nm) and at 607 nm (excitation at 532 nm), as well as the radiation of the Raman vibrational-rotational spectrum scattered by water vapor (Kumar et al., 2011). This channels are not used in the present study.

The Raman Lidar model LR331D400 located in Granada (Raymetrics S.A., Greece) is described in detail by Guerrero-Rascado et al. (2008). It is configured to point vertically to the zenith and based on a pulsed Nd: YAG laser with the fundamental, second and third harmonic generators providing pulses at the same wavelengths as the Barcelona lidar laser. The system emits pulses at 355 nm, 532 nm and 1064 nm with respective energies of 60 mJ, 65 mJ, and 110 mJ at a

repetition rate of 10 Hz. To collect the backscattered radiation it uses a 40-cm diameter Cassegrainian telescope, which focus the light into the polychromator optics directing each wavelength to the corresponding photodetector. The available channels are the same as in the Barcelona system. The optics setup is such that the maximum overlap has reached at above 320 and 420 m (above instrument) for 532/1064 and 355 nm channels, respectively.

During the daytime, the aerosol optical coefficient profiles (backscatter and extinction) at both stations were retrieved by means of the two-component elastic lidar inversion algorithm (Fernald, 1984; Sasano and Nakane, 1984; Klett, 1985) constrained with the sun-photometer-derived AOT.

Satellite images of MODIS and MSG/SEVIRI sensors were used to visualize the geographical distribution of the aerosol plumes. The Hysplit, NAAPS and DREAM models were also used to confirm the origin and the trajectory of the plumes. The models NAAPS and DREAM predict dust intrusions over the investigated area. The Hysplit model provides the trajectories of air masses overpassing the IP.

2.2 Methodology

The NAAPS and DREAM models were used to make the first sight about dust intrusions. After that, the Hysplit 5-day backward trajectories to Granada were used to determine dust intrusion scenarios in this site. Then, in order to investigate the variation of aerosol properties, 5-day forward-trajectories from Granada to Barcelona were computed. Saharan clusters sources were estimated performing cluster analysis of Hysplit trajectories.

In order to discriminate dust from other different aerosol types, the method of Gobbi et al. (2007) is used. Here the spectral dependence of the Ångström exponent $\delta\alpha$ defined as the difference of Ångström exponent values $\delta\alpha = AE_{440\text{-}675} - AE_{675\text{-}870}$ was taken into account. The use of Gobbi plots permit to get additional information about the contribution of fine and coarse modes to AOD (Fig. 1). This method infers about the AOD increase, caused by fine particle humidification or by the increase of the presence of coarse particles. The use of the spectral dependence of the Ångström exponent curvature give more insight on separating fine and coarse mode contributions to AOD (O'Neill et al. 2001a). Basart et al. (2009) found that under the dominance of coarse mode aerosol, such as desert dust, $\delta\alpha$ tends to be negative or slightly positive (between −0. 3 and 0.1). Thus, according to Basart et al. (2009), the days associated by $AOD_{675}>0.15$, $AE_{440\text{-}870}<0.75$ and $-0.3<\delta\alpha<0.1$, are considered as days with coarse mode domination. The days in which $AOD_{675}>0.15$ and $AE_{440\text{-}870}<0.75$, but $\delta\alpha>0.1$, are considered as days with the bimodal pattern. In the last case, both fine and coarse modes contribute to AOD (Valenzuela et al., 2012). Meanwhile days with the same conditions, but with $\delta\alpha<-0.3$ are dominated by the fine mode. The plots α - $\delta\alpha$ from AERONET data, classify dusty days into two categories: dusty days with coarse mode domination and dusty days with bimodal patterns.

In the case of missing AERONET data (as in the case of August 2012), data of aerosol optical depth and Ångström exponent are taken from MODIS products. After that, the aerosol optical data at the two stations are compared between them.

Dust events are considered the period of several consecutive dusty days. Thus, the number of dusty days per dust event and their statistical parameters are estimated. A cluster analysis for Hysplit 5-days back-trajectories from 1 km up to 6 km was performed. These analyses determine the origins and the pathways of dust intrusions over Barcelona and Granada during the period June-September. Several distributions of the number of back-trajectories are computed, based on the cluster origins and the pathways of Saharan dust intrusions.

Another important step of our analysis is the estimation of aerosol optical properties and their differences during dust events at both stations. These analyses were performed during the coincidence of dust events at both stations. The principal optical parameters investigated, AOD_{675} and $AE_{440\text{-}780}$, are classified according to the dust intrusion scenarios. These parameters are also monthly averaged and subsequently compared between the two stations.

In order to better compare the optical parameters derived from the lidar measurements, we have computed the transport time of dust from Granada to Barcelona in coincident dusty cases. To do this, Hysplit forward-trajectories departing from Granada with 6hr resolution are used. These trajectories depart at the heights of 2, 3, 4, 5 and 6 km. Time-transport of air masses was estimated as the time required by of HYSPLIT trajectories to overpass both stations. After this, the comparisons of the optical properties of the same plumes when they overpass each station were performed.

3. Dust event characteristics and statistics at both stations

3.1 Dusty day analysis

Aerosol optical properties during dust events are analyzed using the data of AERONET for Aerosol Optical Depth (AOD_{675}), Ångström exponent ($AE_{440\text{-}870}$) and the wavelength dependence of Ångström exponent ($\delta\alpha$). The criteria to discriminate the dusty days are as follows; $AOD_{675}>0.15$, $AE_{440\text{-}870}<0.75$ and $-0.3<\delta\alpha<0.1$. Fig. 1 presents the measurement results on a Gobbi plot during the investigated period in Barcelona and Granada.

The numbers of the dusty days are presented in table 1. This analysis revealed that during the eight-month period June-September, 2012-2013, 23 dusty days are obtained in Barcelona and 64 in Granada. Percentiles of all dusty day at each site are then computed for each month.

According to these data, dust events are more frequent in August, by 52.2% in Barcelona and 39.1% in Granada. The second most affected month by dust events at each station was June, by 21.7% in Barcelona and 28.1% in Granada. But, surprisingly, July was affected less than June by

dust events. This fact was observed at both sites, but especially at Barcelona site. The number of dusty days during July counts of 8.7% and 23.4% of the total number of dusty days, in Barcelona and Granada respectively. Meanwhile, the fractions of dusty days in September were 17.4% and 9.4%, in Barcelona and Granada respectively.

Because of its geographical position, Barcelona is expected to be affected less than Granada by dusty events. This site can be more influenced by continental pollution and marine aerosols. The modes of their distributions were located in August, where are retrieved their distribution peaks. The correlation coefficient between the numbers of dusty days at these stations over each month was high, 0.81. High values of the correlation coefficients indicate that the dust events over Barcelona and Granada may be related to the same dust intrusions over the Iberian Peninsula (IP). Nevertheless, the more detailed analysis of back-trajectories gives more explanations over these dust intrusion scenarios over the IP.

3.2 Dust events analysis

Besides the dusty day analysis, also the dust events are analyzed. Taking into account the previous consideration, several dust events in the investigated period are evidenced. It is important to take into account that several dust events span over two consecutive months. This fact is taken into consideration during analysis of dust events during each month. The total number of dust events was 10 and 22, respectively in Barcelona and Granada. The statistical distribution of numbers of dusty days per each dust event, in Barcelona and Granada, is presented in Fig. 2. The distribution of dusty days per dust events in Barcelona does not have any peak. It looks like a uniform distribution in the range 1-3 dusty days per dust events. However, this distribution in the case of Granada has a distinct mode, on the value 2.

The mean values of the number of dusty days per dust event are 2.3 and 2.9 respectively in Barcelona and Granada. The standard deviation was found to be correspondingly 1.25 and 2.04. Thus, the average duration of a dust event was found to be not too much different at two sites. The durations of the dust events range up to five days in Barcelona and up to eight days in Granada. Also, the dust event duration in each month does not differ too much from Barcelona to Granada. These results allow us to investigate the duration of dust events in each month, taking into account both stations at the same time. So, the average duration of dust events at both sites was: 3.0, 2.0, 4.1 and 1.4 for June, July, August, and September. Thus, in August, not only occurs the major number of dust intrusions over the IP, but also the longest one.

It must be taken into account another important factor, which influences the distributions of dusty days at both sites. The numbers of dusty days at both sites (taken together) are 64 and 23 in 2012 and 2013 respectively, which indicates that the IP was affected by Saharan dust intrusions more intensively in 2012 than in 2013.

4. Dust intrusion scenarios over Barcelona and Granada sites; origins and pathways

In order to have a clear picture of the main scenarios of dust intrusions over Barcelona and Granada sites, 5-day HYSPLIT backward trajectories are used, from 1 km to 6 km a.g.l., with a vertical resolution of 1000 m.

Backward trajectories analyses suggest three clusters over Saharan desert, which are the main contributors to dust intrusions over Barcelona and Granada, similarly to the scenarios described by Escudero et al. (2005) and Valenzuela et al. (2012). Our clustering analysis reveals a pathway from south to north, mainly in emission areas in Morocco and west of Algeria (cluster A), a pathway from west via an Atlantic arch with emission areas over West Sahara, Mauritania, south of Algeria and north of Mali (cluster B) and a pathway from east across the Mediterranean sea with emission areas over the remaining part of Algeria and Tunisia (cluster C).

Cluster A has the major contribution at both stations (more than the half of all back trajectories in both stations), whilst cluster C has the minor contribution in both stations. Anyway, some differences between their contributions are found. The percentiles of the contributions of cluster A and C are higher in Barcelona, whilst cluster B contributes more in Granada.

However, the vertical distribution within each cluster is different. Interestingly, the highest contributions in cluster A are encountered at 5-6 km altitudes over Barcelona and in 3-6 km over Granada (Fig. 3.a.), as a consequence of the impact of the Atlas Mountains orography driving air masses to higher altitudes during their travel to the Iberian Peninsula. In contrast, clusters B and C are more uniformly distributed at both stations in altitude due to a less impact of the westernmost and easternmost branches of Atlas Mountains on the pathways.

The different pathways followed by the dust intrusions were also analyzed. The main pathways are the Atlas Mountains (for both stations) and Atlantic arch (especially for the Granada station) (table 2), accounting for ~62% and ~38% of Barcelona site, and ~54% and ~46% of Granada site. Saharan air masses affecting both stations mainly overpassed the Atlas Mountains. Figure 3.b. shows in detail the different pathways at each altitude. Back-trajectories overpassing the Atlas Mountains reach Barcelona at all altitudes, with a maximum in the height levels 5 and 6 km, and with a relevant contribution of 2 and 3 km. Similarly, the Atlantic arch back-trajectories arrive at Barcelona, mainly at the height levels 5 and 6 km. In contrast, the pathway vertical distribution of backtrajectories reaching Granada crossing the Atlas Mountains shows marked differences respect to the Barcelona distribution, with relevant contributions at all the analyzed levels above 3 km (maximum at 4 km-level) as a consequence of this orographic barrier acting as a springboard injecting mineral dust particles at altitudes above their summits. Due to the relatively short distance to the Granada station, subsidence processes cannot have enough time to act and mineral dust particles keep confined at high altitudes. In contrast, the Atlantic air masses arrive in Granada almost at all altitudes. The comparison between the patterns of Fig. 3.a. and 3.b. reveal that the Atlas back-trajectories in Granada are negligible at 1 km and intensive at 4

km. The Atlantic back-trajectories have more similar altitude distributions. Taking into account the cluster and pathway analysis, several scenarios of dust intrusion over Barcelona and Granada occurring during the period June-September have been identified: scenario I (cluster A with pathways through the Atlas Mountains), scenario II (cluster C with pathways through the Atlas Mountains), scenario III (cluster B with Atlantic arch pathway), scenario IV (cluster A with Atlantic arch pathway) and scenario V (remaining scenarios).

Figure 3.c. presents the percentage of the contributions of the different scenarios at both stations. According to our analysis, air masses overpass Barcelona, mainly at altitudes 2-6 km (scenario I), 1-2 km (scenario II), 5-6 km (scenario III) and 5 km (scenario IV). It is worthy to note that the contribution of scenario II at lowest altitude while other scenarios contribute more at highest altitudes. Scenario IV is the predominant scenario of dust intrusions in Granada at 3, 4 and 5 km, with a relevant predominance of scenarios I (at 3 km) and III (3 and 5 km). Meanwhile, the scenario II has the lowest contribution.

Some differences in dust intrusion scenarios are observed between Granada and Barcelona. The major difference in their contribution was observed in the case of scenarios II and III. The percentile contribution of the scenario II is 1.9 times higher in Barcelona than in Granada, whilst scenario III is 2.3 times lower. Other scenarios differ less than the above two at the two stations.

5. Columnar aerosol properties during dust events at both stations

Series AOD_{675} and $AE_{440,870}$ indicate some features of the aerosol properties in Barcelona and Granada in the periods June-September 2012 and June-September 2013 (Fig. 4). The combination of the information about AOD and AE gives the first sight of the relevance of the dust events at two sites. Moreover, about 95.3% of daily averaged AOD_{675} during the dust events falls in the interval 0.15-0.75. Exceptions are found only in three cases, exceeding the value 1.0 (two in Granada and one in Barcelona). $AE_{440-870}$ at both stations is mainly in the interval 0.0-0.8 (97.6%), with values generally higher in Barcelona than in Granada.

At the Barcelona site, two distinct groups of aerosols were identified, characterized by 0.10 μm $<R_f<$ 0.20 μm with $\eta<30\%$ and 0.10 μm $<R_f<$ 0.20 μm with $50\%<\eta<90\%$. The mean values of AOD_{675} were higher in the first situation compared to the second one. In the first situation values of $\delta\alpha$ were close to zero or slightly positive (up to 0.25), indicating a strong contribution of coarse mode to AOD. In the second situation, the values of $\delta\alpha$ ranged from slightly positive to negative (usually higher than -0.3). In this case, both fine and coarse modes are expected to contribute to the total AOD. Taking into account that the mean AOD_{675} in the second situation was lower than in the first one, and in both situations two modes contribute on AOD, we may state that the contribution of the coarse mode in the second situation was very low compared to the first one.

In the case of Granada, the dusty events were characterized by R_f<0.15 μm and η<30%. The values of δα were positive, suggesting the contribution of both modes (fine and coarse) to AOD. Mean values of daily averaged optical properties during all dust events are; AOD_{675} 0.29 and 0.34, respectively in Barcelona and Granada, whilst $AE_{440-870}$ 0.54 and 0.30. These mean values indicate the strong presence of the fine mode aerosols during the dust events in Barcelona in comparison to Granada. In order to estimate the influence of Saharan dust on AOD, the coarse mode contribution on AOD (1-η) during dusty days was analyzed. Figure 5 presents the frequency distributions of 100· (1-η). Coarse modes contribute more than 50% in AOD during all dusty days in Barcelona and Granada. However, some differences of these parameters are found in two stations. Thus, the average values of this contribution were 66.6% and 75.3% in Barcelona and Granada, respectively. Figure 5 indicates that the frequency is lower than 60% for both sites, while the most frequent corse mode contribution to AOD_{675} was 60% and 80%, respectively for Barcelona and Granada.

Figure 6 presents the overall results of average aerosol optical parameters for all dust events in Barcelona and Granada during each month. The average values of AOD_{675} during dusty days in Granada differs slightly from Barcelona (1.2 times higher) and its average $AE_{440-870}$ was found 1.7 times lower.

The mean values of AOD_{675} and $AE_{440-870}$ during the dust events according to several scenarios in Barcelona and Granada (origins and pathways), as well as the mean altitudes where the majority of back-trajectories overpass each station during all dusty days and their frequency, are presented in Table 3. Only scenarios I-IV (containing 94% of all back-trajectories overpassing both stations during their dusty days, have been analyzed.

The scenarios I and II are the most frequent in Barcelona, accounting for 46% and 21% of all back-trajectories overpassing this station. These two scenarios bring air masses in Barcelona with higher AOD (0.30 and 0.35). Air masses of these two scenarios follow the same pathway, overpassing the Atlas Mountains. On the other hand, the scenarios which follow the Atlantic pathway bring air masses with lower AOD (0.25). It was not observed any substantial difference between the AE values according to different scenarios of dust intrusions over Barcelona. Anyway, average AE during scenario IV was slightly higher than the others. High AE values during dust events over Barcelona arise due to the fact that air masses of these scenarios usually move clockwise crossing over entire IP and the northwest Africa, consequently, over many populated areas, enabling to collect fine mode particles from these areas. Overpassing these areas increases the fraction of the fine mode particles and so increasing the Angstrom exponent. In short, air masses which move clockwise from clusters A and C through the Atlas Mountains are the dominant scenarios for dust intrusions over Barcelona.

In the Granada's case, the scenarios I and III are most frequent over Granada (40% and 34%). The scenario I was the most dominant for both stations. Even though scenario I and III are completely different in terms of air masses origins and their pathways, these two scenarios bring

are characterized by the same AOD (0.36) and AE (0.28 and 0.24). In terms of AOD and AE, scenario II presents the most intense dust intrusions over Granada. It is characterized the highest AOD (0.46) and low AE (0.25). But this scenario is not very frequent over Granada (only 11% of all the cases).

The correlation coefficients between the averages of AOD, AE and the average altitude of back-trajectories (h_{avg}) in different scenarios are negative correlations of AOD-AE and AOD-h_{avg}. For all scenarios, the average values of AOD_{675} ($AE_{440-870}$) in Barcelona are lower (larger) than in Granada. The distribution of the average altitude of air masses is similar in two stations. Scenario II brings air masses at lower altitudes at both stations.

In spite of the same scenarios at both stations suggest that the dust events arrive with similar origins and pathways at the two stations, the aerosol optical properties of dusty days during these scenarios differ at these sites. As a consequence of the processes occurred during the transport, a decrease in the mean AOD_{675} is observed, related to the deposition of coarse mode during the pathway from Granada to Barcelona (in cases when the same plume overpasses both sites). Similarly, the increase of mean $AE_{440-870}$ is related to the increase of the anthropogenic particle load (fine mode) in the atmospheric column in Barcelona compared to Granada.

6. Coincident dust events

In this section we focus on dust events spatially and temporally coincident at both sites, i.e. dust plumes transported first over Granada and a few hours later over Barcelona. The days of a coincident dust event must fulfill two criteria: 1) they must be classified as dusty days (see Section 3.1) at both sites, and 2) the back trajectories run from Barcelona, which originates in the Sahara region must also overpass Granada. In total 22 days fulfill both criteria, distributed in 9 dust events:

- 2 dust events in June (of 2 and 3 coincident days),
- 1 dust event in July (of 2 coincident days),
- 4 dust events in August (of 1, 3, 3 and 5 coincident days) and
- 2 dust events in September (of 1 and 2 coincident days).

Among those cases, we selected three events (Fig. 7), which are well documented by sun-photometer simultaneously at both sites: 18 - 19 June 2012 (event I), 27 - 29 June 2012 (event II) and 2 - 6 August 2013 (event III, see Table 4). The three coincident dust events correspond to different scenarios of dust intrusions (see Section 4.3). The dust event I originated mostly from cluster A and reached the IP through the Atlas Mountains (scenario I). Cluster B and more rarely cluster A are the principal sources of the dust event II with trajectories passing through the Atlantic (scenarios III and IV). Cluster B is the principal source of the dust event III with pathways above the Atlantic (scenario III). The analysis of the differences in the dust optical

properties (AERONET-derived AOD675, $AE_{440\text{-}870}$ and coarse mode fraction, *CMF*, Table 4) between both sites for each of those dust events is expected to give valuable information about the influence of the transport processes on these properties. A straightforward (and expected) finding from Table 4 is that in all dust events AOD_{675} decreases from Granada to Barcelona (-0.11 to -0.01) while $AE_{440\text{-}870}$ increases (+0.16 to +0.34) and *CMF* decreases (-0.18 to -0.09).

In order to illustrate how the coincident dust events were defined, we show in Fig. 8 some of the tools used to classify event I (18-19 June 2012) as a coincident dust event. The observed daily OMI aerosol index shown for 19 June confirms the presence of dust at both sites, which is forecasted by both maps of NAAPS and DREAM dust AOD at 550 nm shown for 19 June at 12 UT. The superimposed wind direction at 3 km on the DREAM map also indicates that the dust transport direction in Granada is likely northeastward, i.e. in the direction of Barcelona. Hysplit back trajectories arriving in Barcelona on 19 June at 12 UT at 4 and 5 km are overpassing the region of Granada and are originating in the Sahara region. The back trajectory arriving at 3 km also comes from the Sahara region, but does not overpass Granada.

6.1 Optical properties vs. transport paths

In order to better analyze the differences of the dust optical properties during the three coincident events, we first examine the time of dust transport from Granada to Barcelona and the predominant height of transport at each site. The time of dust transport, defined as the time required for a dust plume to travel from Granada to Barcelona, was determined with 3hr time resolution Hysplit forward-trajectories departing from Granada at heights of 2, 3, 4, 5 and 6 km and run every 6 hours. Each time a forward-trajectory from Granada overpasses Barcelona, the time of dust transport between the two stations was calculated by the estimation of time-transport of the Hysplit trajectories with 3hr time resolution. It is worth saying a word about the patterns observed (but not shown) of the forward-trajectories between Granada and Barcelona during the three coincident dust events. The trajectories have very similar shapes usually overpassing eastern Spain and its Mediterranean coast. However, we observed little differences between events, I and II and event III: while the trajectories during events I and II are relatively straight and travel over land, they are slightly curved and travel partly over the Spanish Mediterranean coasts during event III. The trajectories of the air masses during dust event III pass also along the urban centers in the north Spanish Mediterranean coasts which are more populated than those which are overpassed by the trajectories in the inland. Thus, mixing process of the dust plumes with anthropogenic aerosols is more frequent during the dust event III compared to the other two dust events. This slight difference between events I and II and event III might be an explanation of the high values of $AE_{440\text{-}870}$ (0.53, Table 4) and the low values of *CMF* (0.63) observed in Barcelona during dust event III. This first result emphasizes the importance of the activities in terms of aerosol formation in the regions over which the dust is transported, which can, in the case of mixing, modify the dust plume optical properties. Fig. 9 shows the temporal mean of the dust transport time as a function of height for the three coincident dust events. The mean values of the dust transport time from Granada to Barcelona taking into account all altitudes in the 2–6

km range are 15.8, 11.2 and 14.3 hours for dust event I, II and III, respectively. Shorter transport times are due to a stronger atmospheric dynamics and thus to more marked synoptic conditions, which favor the potential aerosol mixing (Kok et al., 2012). On the other hand, shorter transport times don't allow any substantial AOD change. The case with the shortest transport time, dust event II, also corresponds to the case with the extreme changes of the aerosol parameters (Table 4); lowest variations of the AOD (-0.01), and the highest variation of the Ångström exponent (+0.34) and of the coarse mode fraction (-0.18). All the three dust events have almost the same pattern of the altitude profile; both decreasing with respect to the altitude. Dust events I, II and III decrease from 24.3, 16.9 and 21 at 2 km a.g.l. to 10.4, 8.3 and 10.2 at 6 km a.g.l. The time required for a dust plume to be transported from Granada to Barcelona depends on many factors and especially on wind speed, which itself depends on altitude. Generally, the transport time is longer at low altitude and decreases with increasing altitude (Heinzerling, 2005). This behavior of the transport time is found during all the three dust events for which the correlation coefficients of the transport time vs. height are very high: -0.96, -0.89 and -0.95.

In addition to the type of scenario of each dust intrusion, the region overpassed and the transport time, the altitude of the transport can also contribute to modifying the dust optical properties during their transport from Granada to Barcelona. To estimate the transport height of each dust event at both sites, we have used 6-hour time resolution Hysplit back trajectories arriving in Granada and in Barcelona at heights of 2, 3, 4, 5 and 6 km and run every 6 hours. Only the trajectories originating in the Sahara region were considered in the counting. Fig. 10 shows the percentage per height of trajectories which have their origin in the Sahara region and for the three dust events. Since we have considered five heights, if the same number of back trajectories originating in the Sahara region is found at all heights, then the percentage is 20 % at all heights. No strong differences are observed between both stations and between the dust events. During dust event I, the largest number of trajectories originating in the Sahara region occurs at 3 and 4 km in Granada and at 2 and 3 km in Barcelona. During dust event II and III, the largest number of trajectories originating in the Sahara region occurs at 3-4 km and 3-4-5 km, respectively, independently of the stations. The most evident changes between both stations are:

- During dust event I the altitude differences level off: while the number of trajectories at 4 and 5 km decreases (from Granada to Barcelona), it increases at 2 and 6 km. The range of the percentage of trajectories passes from [2.5; 32.5 %] (30-% variation) in Granada to [12.5; 23.2 %] (10.7-% variation) in Barcelona. The number of trajectories originating in the Sahara region at 6 km in Granada is multiplied by a factor 5 in Barcelona.
- During dust event II the decrease (from Granada to Barcelona) at 6 and 3 km is related to an increase at 5 and 2 km, respectively. The range of the percentage of trajectories passes from [13.4; 26.9 %] (13.5-% variation) in Granada to [12.5; 25.0 %] (12.5-% variation) in Barcelona.
- During dust event III, the amplitude relationship approximately maintains. The highest number of trajectories originating in the Sahara region occurs at 3-4-5 km.

From this analysis, it appears that the capability of the dust layers to spread vertically along their transport from Granada to Barcelona is linked to the dynamics conditions: the stronger the dynamics, the more the layers will extend vertically (dust event I). Dust event III is a clear example of a low dynamics which results in an insignificant modification of the dust layer vertical extension.

The temporal evolution of the dust optical properties (AERONET-derived AOD_{675}, $AE_{440\text{-}870}$, and coarse mode fraction) is shown in Fig. 11, in which the gray areas indicate the coincident events. One sees that the AOD temporal evolution is highly correlated with the coarse mode fraction. In terms of AOD, dust event II is the strongest (maxima of 0.82 and 0.76 in Granada and Barcelona, respectively) while dust event III is the weakest (maxima of 0.41 and 0.34, respectively). The same conclusions can also be drawn from the average values of Table 4. In terms of duration, dust event III is the longest while dust event I is the shortest. The event duration is correlated with the dust transport time from Granada to Barcelona found earlier (15.8, 11.2 and 184.3 hours on average over all considered heights for dust event I, II and III, respectively): the shorter the transport time, the shorter the duration of the event. Because strong atmospheric dynamics (dust event I) favors the suspension of the particles and prevents (or reduces) potential aerosol mixing, one would expect a stronger signature of mineral dust during the dust event I. However, the lowest values of $AE_{440\text{-}870}$, an indicator of the dust "purity", are observed during dust event II (average values of 0.11 and 0.45 in Granada and Barcelona, respectively). This result points out that the dust during dust event I probably arrived over the IP already mixed with other aerosol types (the largest $AE_{440\text{-}870}$ in Granada, +0.34, is found for dust event II) and that further mixing was low or inexistent between Granada and Barcelona (the lowest $AE_{440\text{-}870}$ difference, +0.16, is found for dust event I).

The AOD increase in Barcelona is much closer in time to the AOD increase in Granada during dust event I than during the other two events. While the AOD and *CMF* evolution during dust event I and III are similar in shape at both sites, during dust event II differences are observed: the gradual AOD decrease in Granada is also observed in the coarse mode fraction in Granada and in Barcelona (Fig 11.c) but not on the AOD in Barcelona, which remains approximately constant and decreases at the end of the event more abruptly. From Table 4, one sees that during dust event II the AOD remains roughly constant between Granada and Barcelona while the $AE_{440\text{-}870}$ increase (+0.34) and the *CMF* decrease (-0.18) are the strongest. These results point out that the decrease in the contribution of the dust large particles to the total AOD between Granada and Barcelona was somehow compensated by the increase of the contribution of new and finer particles in Barcelona. At this point, further investigation is needed to characterize these new fine particles. In summary of this Section:

- Dust event I (scenario I) can be classified as a moderate event of a short duration (< 3 days) and characterized by a strong atmospheric dynamics with similar intensive parameters ($AE_{440\text{-}870}$ and *CMF*) in Granada and in Barcelona.

- Dust event II (scenario III and IV) is a moderate-to-strong event with quasi-pure mineral particles in Granada and characterized by the largest difference between Granada and Barcelona intensive parameters. The strong increase of the $AE_{440\text{-}870}$ and decrease of *CMF* between Granada and Barcelona lets think to an increase contribution of fine particles between both sites.
- Dust event III (scenario III) is a low-to-moderate event of a long duration (> 5 days) and characterized by a low atmospheric dynamics (long transport times) which favors the falling of larger particles by sedimentation (low *CMF*).

6.2 Evolution of the dust vertical distributions during dust event III

After looking at the Section 6.1 at the statistical transport heights estimated by backward trajectories, we now look at the vertical distribution of the dust plumes measured by lidar at both sites. The availability of lidar measurements simultaneously at both sites does not allow performing such an analysis during dust events I and II. Thus, we focus here only on dust event III. The lidar systems are those described in Section 2.1. Fig 12 shows 30-min. averaged profiles of the backscatter coefficient at 532 nm obtained in Granada and Barcelona during the period 1 – 6 August 2013. According to Fig 10, the dust time transport during dust event III was, on average, on the order of 17 - 24 hours (~1 day) at the altitude of 2 km up to 8 - 10 hours (one-third of a day) at the altitude of 6 km. For that reason, in Fig. 11, the Barcelona profiles are displaced in time by 12 – 24 hours with respect to the plots of Granada. When on a given day, no profiles are shown for a station, it simply means no lidar measurements are available on that day. The few data available at the Barcelona station only allow a direct comparison with two cases. Note that although 1 August is outside of the period of dust event III (2-6 August) because no dust was detected in Barcelona on that day, it is considered in this section in order to make the spatio-temporal comparison between Granada (1 August) and Barcelona (2 August).

From the temporal evolution of the profiles of the backscatter coefficient in Granada, it results that the top of the dust layer is quite stable during the whole event: it is around 6.8 km on 1 August and oscillates between 5.7 and 6.3 km during 2-6 August. The vertical structure of the dust plume is rather uniform in the middle of the event (2-4 August): shallow vertical variations are observed especially on 2 and 4 August. In the middle of the event, the backscatter coefficient between 2 and 5.5 km has a mean value of 0.73 $Mm^{-1}\cdot sr^{-1}$ on 2 August and of ~1.50 $Mm^{-1}\cdot sr^{-1}$ on 3 and 4 August. The vertical structure and the values of the backscatter coefficient found in the dust plume are comparable to a former event observed in Granada in 2005 and documented in Guerrero-Rascado et al. (2008). In Granada the profiles shown do not allow saying if the dust plume is coupled or decoupled from the planetary boundary layer (PBL) which in Granada is on average around 1.6 km a.s.l. in summer (Navas-Guzmán et al., 2013). The Barcelona system presents the peculiarity of pointing not at the zenith but at 52º off zenith, which allows decreasing significantly the useful height of the profile, in addition to the fact that Barcelona is closer to sea level than Granada (125 vs. 680 m a.s.l.). This advantage, clearly shown in the two

plots of the Barcelona data, allows retrieving the PBL height in Barcelona, which is around 1.3 and 1.2 km on 2 and 5 August, respectively. In both cases, the dust layer in the free troposphere is clearly decoupled from the PBL. Such a PBL height is in the higher range of the statistical values [0.30 – 1.45 km] found by Sicard et al. (2006) in Barcelona over a 3-year time period. The Ångström exponent in Barcelona is also a clear indication of the decoupling between the PBL and the lofted dust plume since it is higher than 1 in the PBL (excepting overlap effect for heights < 0.5 km) and lower than 1 in the dust plume. In Granada the Ångström exponent shows always the same tendency with height: it decreases with increasing height. It starts at values between 1 and 2 in the bottom part of the profiles (usually near 1.5 km) to values near 0 and even negative (-0.2) on 3 and 4 August in the top part of the profile (above 3 km). We find a good agreement with the results found in the previous section for dust event III: shorter transport time at a higher altitude, which favors the suspension of the particles and a higher number of trajectories originating in the Sahara region at 3-4-5 km. These results indicate a higher level of "purity" of the mineral dust at higher altitude and therefore a lower Ångström exponent. In terms of temporal evolution, we can distinguish two different periods: 1 - 2 August when the Ångström exponent between 2 and 5.5 km has a mean value of 0.51 - 0.65 and 3 - 6 August when its mean value is lower and around 0.09 - 0.32.

The profile of the backscatter coefficient in Granada on 1 August at 14 UT is compared to that in Barcelona 18 hours later, on 2 August at 08 UT. If we discard the cloud at 6 km present in the Granada profile, the two profiles are very similar in shape. The correlation coefficient calculated between both profiles between 2 and 5.5 km is 0.63. The mean backscatter coefficient between 2 and 5.5 km is higher in Barcelona ($\bar{\beta}$=0. 97) than in Granada ($\bar{\beta}$=0.76). The profile of the backscatter coefficient in Granada on 4 August at 14 UT is compared to that in Barcelona 24 hours later, on 5 August at 14 UT. The profiles are very similar in the top part of the plot (> 3.5 km). Below 3.5 km the profiles start to diverge: while the Granada profile increases (with decreasing height), the one of Barcelona has a general tendency to decrease. This difference produces a mean backscatter coefficient between 2 and 5.5 km higher in Granada ($\bar{\beta}$=1. 46) than in Barcelona ($\bar{\beta}$=1.29). It also makes the correlation coefficient drop to a value of 0.21. At this point, we do not know the origin of that difference, but two hypotheses can be formulated: a local aerosol load lower in Barcelona than in Granada or a dust load in the bottom part of the profiles [1 – 3 km] lower in Barcelona than in Granada. A combination of both hypotheses is also possible. According to the work of Sicard et al. (2006) in Barcelona and Navas-Guzmán et al. (2013) in Granada, the PBL in summer may extend vertically up to higher altitudes in Granada (~2 km) than in Barcelona. Given the similarities between the number of back trajectories originating in the Saharan region arriving at 2 km in Granada and Barcelona (Fig. 10), it is possible that the difference between the profiles of the backscatter coefficient in Granada (4 August) and Barcelona (5 August) in the 1.5 – 3 km range might be due to different local aerosol load. The higher Ångström exponent in Granada in that range (compared to the 3-6 km range) also supports the hypothesis of a mixing of dust with local aerosols.

7. Conclusions

Statistical analyses of the characteristics of dust intrusion properties at two EARLINET sites in Spain were performed. For this purpose, we have investigated the period June-September during the years 2012 and 2013.

There are detected 10 dust events (23 dusty days) in Barcelona and 22 dust events (64 dusty days) in Granada. August was the month most affected by Saharan dust intrusions, having about 52.2% of the total dusty days in Barcelona and 39.9% in Granada. There are identified also 22 coincidence cases affecting both stations.

Cluster analyses of Hysplit backward trajectories reveal that there are three main source regions of Saharan dust affecting the IP; Morocco and west of Algeria (cluster A), West Sahara, Mauritania, south of Algeria and north of Mali (Cluster B), remaining part of Algeria and Tunisia (cluster C). At Cluster A originates the majority of the dust outbreaks; 61% of the events affecting Barcelona and 53% affecting Granada.

The majority of backward trajectories come through Atlas Mountains; 62.4% and 54.1% respectively at Barcelona and Granada sites, while the other backward trajectories come through Atlantic.

The principal scenarios of dust intrusion in Granada originate from cluster A (and B) and come through Atlas Mountains (Atlantic). Meanwhile, in Barcelona, dust intrusions usually originate in cluster A and come through the Atlas Mountains.

Despite the differences, according to the dust intrusion scenarios, the majority of Saharan backward trajectories overpass Barcelona and Granada at 3-6 km, during their dust events. The presence of the Atlas Mountains complicates the passage of air masses over Granada at lowest altitudes.

More detailed analyses estimate the aerosol optical properties during dust events. Mean values of AOD_{675} and $AE_{440\text{-}870}$ are; 0.29 and 0.54 in Barcelona, and 0.34 and 0.30 in Granada. The dust intrusions from cluster A through the Atlas Mountains are the most frequent over the two sites. This scenario brings air masses with high AOD in Barcelona (0.30) and in Granada (0.36). Meanwhile there are identified strong differences between AE values at both stations during this scenario. Mean AE during this scenario, are 0.53 and 0.28, for Barcelona and Granada respectively. The increment of AE during the transport process from Granada to Barcelona is related to two main processes; deposition of coarse mode aerosols and contamination by fine mode anthropogenic products. $AE_{440\text{-}870}$ was more affected by the time transport of air masses, while AOD_{675} don't show any significant difference. Anyway, the differences of optical properties between two sites are affected more by the shape of the trajectories than by time duration.

Mean time-transport of Saharan dust from Granada to Barcelona were estimated 11 - 14 hours, depending on the pathway of the dust intrusion and the heights of back-trajectories. During the dust transport from Granada to Barcelona, AOD_{675} undergoes only little changes. Angstrom exponent in Barcelona is 1.35 times greater than in Granada during the mineral dust events. Thus, the transport process is associated with the contamination by fine mode aerosols, produced primarily by anthropogenic activities in the region of IP. Also, the mean altitude of back-trajectories decreased during this transport. Time plots of optical parameters during the coincidence dust events have almost the same pattern for both sites, with Barcelona's plots postponed by time-transport of the dust plume. This fact confirms the approximate origin of these dust events in these sites.

Lidar profiling of backscatter coefficients offered another point of view of the evolution of dust events at these sites. The patterns of bsc_532 nm during the coincidence dust events in Barcelona and Granada indicated clearly the evolution of the dust events and the transport process in these two sites. The Ångström exponent in Barcelona is higher than 1 in the PBL and lower than 1 in the dust plume. In Granada the Ångström exponent shows always the same tendency with height: it decreases with increasing height from 1-2 in the bottom part of the profiles to values near 0 and even negative in the top part of the profile. The profiles of the backscatter coefficient in Granada were compared to that in Barcelona 18 hours later. The correlation coefficient calculated between both profiles between 2 and 5.5 km is 0.63.

Acknowledgments

Lidar measurements in Granada and Barcelona were supported by the ACTRIS (Aerosols, Clouds, and Trace Gases Research Infrastructure Network) Research Infrastructure Project funded by the European Union's Horizon 2020 research and innovation program under grant agreement no. 654169 and previously under grant agreement no. 262254 in the 7th Framework Programme (FP7/2007-2013). Measurements in Granada were also supported by the Andalusia Regional Government through the project P12-RNM-2409 and by the Spanish Ministry of Economy and Competitiveness through the project CGL2013-45410-R. The authors thankfully acknowledge the EFRD (European Fund for Regional Development) program for the instrumentation used in this work. Measurements in Barcelona were also supported by the Spanish Ministries of Economy and Competitivity (projects TEC2012-34575 and TEC2015-63832-P) and of Science and Innovation (project UNPC10-4E-442) and EFRD, and by the Department of Economy and Knowledge of the Catalan autonomous government (grant 2014 SGR 583). This work was supported also by the JoinEU-SEE Erasmus Mundus Partnerships Action 2, which enabled the coordination between the authors of the these research institutions.

References

Alados-Arboledas, L., Lyamani, H. and Olmo, F. J., 2003. Aerosol size properties at Armilla, Granada (Spain). Q. J. Roy. Meteorol. Soc. 129, 1395–1413.

Alados-Arboledas, L., Alcantara, A., Olmo, F. J., Martınez-Lozano, J. A., Estelles, V., Cachorro, V., Silva, A. M., Horvath, H., Gangl, M., Diaz, A., Pujadas, M., Lorente, J., Labajo, A., Sorribas, M., and Pavese, G., 2008. Aerosol columnar properties retrieved from CIMEL radiometers during VELETA 2002, Atmos. Environ., 42, 2654–2667.

Barnaba, F., and Gobbi, G. P., 2004. Aerosol seasonal variability over the Mediterranean region and relative impact of maritime, continental and Saharan dust particles over the basin from MODIS data in the year 2001, Atmos. Chem. Phys., 4, 2367– 2391.

Cachorro, V. E., Duran, P., Vergaz, R., and de Frutos, A. M., 2000. Measurements of the atmospheric turbidity of the north-centre continental area in Spain: spectral aerosol optical depth and Ångström turbidity parameters, J. Aerosol Sci., 31, 687–702.

Cachorro, V. E., Toledano, C., Prats, N., Sorribas, M., Mogo, S., Berjon, A., Torres, B., Rodrigo, R., de la Rosa, J., and De Frutos, A. M., 2008. The strongest desert dust intrusion mixed with smoke over the Iberian Peninsula registered with sun photometry, J. Geophys. Res., 113, D14S04.

Dıaz, A. M., Garcıa, O. E., Dıaz, J. P., Exposito, F. J., Utrillas, M. P., Martınez-Lozano, J. A., Alados-Arboledas, L., Olmo, F. J., Lorente, J., Cachorro, V., Horvath, H., Labajo, A., Sorribas, M., Vilaplana, J. M., Silva, A. M., Elias, T., Pujadas, M., Rodrigues, J. A., and Gonzalez, J. A., 2007. Aerosol radiative forcing efficiency in the UV region over southeastern Mediterranean: VELETA2002 campaign, J. Geophys. Res., 112, D06213.

Eck, T. F., Holben, B. N., Reid, J. S., Dubovik, O., Smirnov, A., O'Neill, N. T., Slutsker, I., and Kinne, S., 1999. Wavelength dependence of the optical depth of biomass burning, urban, and desert dust aerosols, J. Geophys. Res., 104, 31 333–31 349.

Elias, T., Silva, A. M., Belo, N., Pereira, S., Formenti, P., Helas, G., andWagner, F., 2006. Aerosol extinction in a remote continental region of the Iberian Peninsula during summer, J. Geophys. Res., 111, D14204.

Escudero, M., Castillo, S. Querol, X. Avila, A. Alarcón, M. Viana, M. Alastuey, A. Cuevas, E. and Rodríguez, S., 2005. Wet and dry African dust episodes over eastern Spain, J. Geophys. Res., 110, D18S08.

Esposito F., Leone, L., Pavese, G., Restieri, R., and Serio, C., 2004. Seasonal variation of aerosol properties in South Italy: a study on aerosol optical depths, Ångström turbidity parameters and aerosol size distributions, Atmos. Environ., 38, 1605–1614.

Fernández-Gálvez, J. Guerrero-Rascado, J.L. Molero, F. Lyamani, H. Revuelta, M.A. Navas-Guzmán, F. Sastre, M. Bravo-Aranda, J.A. Fernández, A.J. Granados-Muñoz, M.J. Gómez-Moreno, F.J. Olmo, F.J. Pujadas, M. Alados-Arboledas L. 2013. Aerosol size distribution from inversion of solar radiances and measured at ground-level during SPALI10 campaign. Atmos.Res. 127, 130-140.

Formenti, P., Andreae, M. O., Andreae, T. W., Galani, E., Vasaras, A., Zerefos, C., Amiridis, V., Orlovsky, L., Karnieli, A., Wendisch, M., Wex, H., Holben, B. N., Maenhaut, W., and Lelieveld, J., 2001. Aerosol optical properties and large-scale transport of air masses: Observations at a coastal and a semiarid site in the eastern Mediterranean during summer 1998, J. Geophys. Res. 106(D9), 9807–9826.

Gerasopoulos, E., Andreae, M. O., Zerefos, C. S., Andreae, T. W., Balis, D., Formenti, P., Merlet, P., Amiridis, V., and Papastefanou, C., 2003. Climatological aspects of aerosol optical properties in Northern Greece, Atmos. Chem. Phys., 3, 2025–2041.

Guerrero-Rascado, J. L. Ruiz, B. Alados-Arboledas, L., 2008. Multi-spectral Lidar characterization of the vertical structure of Saharan dust aerosol over southern Spain. Atmospheric Environment, 42(11), 2668-2681.

Guerrero-Rascado, J. L. Olmo, F. J. Aviles-Rodriguez, I. Navas-Guzman, F. Perez-Ramirez, D. Lyamani, H. and Alados Arboledas, L. 2009. Extreme Saharan dust event over the southern Iberian Peninsula in September 2007: active and passive remote sensing from surface and satellite, Atmos. Chem. Phys., 9, 8453–8469.

Kinne, S., M. Schulz, C. Textor, S. Guibert, Y. Balkanski, S.E. Bauer, T. Berntsen, T. Berglen, O. Boucher, M. Chin, W. Collins, F. Dentener, T. Diehl, R. Easter, H. Feichter, D. Fillmore, S. Ghan, P. Ginoux, S. Gong, A. Grini, J. Hendricks, M. Herzog, L. Horrowitz, I. Isaksen, T. Iversen, A. Kirkevg, S. Kloster, D. Koch, J.E. Kristjansson, M. Krol, A. Lauer, J.F. Lamarque, G. Lesins, X. Liu, U. Lohmann, V. Montanaro, G. Myhre, J. Penner, G. Pitari, S. Reddy, O. Seland, P. Stier, T. Takemura, and X. Tie, 2006. An AeroCom initial assessment optical properties in aerosol component modules of global models. Atmos. Chem. Phys., 6, 1815-1834.

Heinzerling, D., 2005. Hysplit trajectory modeling and clustering techniques: computation, error analysis, and applcations, Master Thesis, The University of Texas at Austin.

Kaufman, Y. J., Gitelson, A. Karnieli, A. Ganor, E. Fraser, R. S. Nakajima, T. Mattoo, S. and Holben, B. N., 1994. Size distribution and phase function of aerosol particles retrieved from sky brightness measurements. J. Geophys. Res., 99, 10341–10356.

Kok, J. Parteli, E. Michaels, T. Karam, D., 2012. The physics of wind-blown sand and dust. Rep. Prog. Phys. 75 106901, 72pp.

Jamet, C., Moulin, C., and Thiria, S., 2004. Monitoring aerosol optical properties over the Mediterranean from SeaWiFS images using a neural network inversion, Geophys. Res. Lett., 31, L13107.

IPCC Climate Change 2013, 2013. The Physical Science Basis. The contribution of Working Group I to the Fifth Assessment Report of the Intergovernmental Panel on Climate Change.

Israelevich, P. L., Levin, Z., Joseph, J. H., and Ganor, E., 2002. Desert aerosol transport in the Mediterranean region as inferred from the TOMS aerosol index, J. Geophys. Res., 107(D21), 4572.

Israelevich, P. L., Ganor, E., Levin, Z., and Joseph, J. H., 2003. Annual variations of physical properties of desert dust over Israel, J. Geophys. Res., 108(D13), 4381.

Liu, Z., Omar, A., Vaughan, M., Hair, J., Kittaka, C., Hu, Y., Powell, K., Trepte, C., Winker, D., Hostetler, C., Ferrare, R., and Pierce, R., 2008. CALIPSO lidar observations of the optical properties of Saharan dust: A case study of long-range transport, J. Geophys. Res., 113, D07207.

Lyamani, H., Olmo, F. J., and Alados-Arboledas, L., 2005. Saharan dust outbreak over southeastern Spain as detected by sun photometer, Atmos. Environ., 39, 7276–7284.

Lyamani, H., Olmo, F. J., Alcantara, A. and Alados-Arboledas, L., 2006a. Atmospheric aerosols during the 2003 heat wave in southeastern Spain II: microphysical columnar properties and radiative forcing. Atmos. Environ. 40, 6465–6476.

Lyamani, H., Olmo, F. J., Alcantara, A. and Alados-Arboledas, L., 2006b. Atmospheric aerosols during the 2003 heat wave in southeastern Spain I: spectral optical depth.Atmos. Environ. 40, 6453–6464.

Lyamani, H., Olmo, F. J., and Alados-Arboledas, L., 2008. Light scattering and absorption properties of aerosol particles in the urban environment of Granada, Spain, Atmos. Environ., 42, 2630–2642.

Mona, L., Amodeo, A., Pandoolfii, M., Pappalardo, G., 2006. Saharan dust intrusions in the Mediterranean area: Three years of Raman lidar measurements. Journal of Geophysical Research, 111, D16203.

Moulin, C., Lambert, C. E., Dayan, U., Masson, V., Ramonet, M., Bousquet, P., Legrand, M., Balkanski, Y. J., Guelle, W., Marticorena, B., Bergametti, G., and Dulac, F., 1998. Satellite climatology of African dust transport in the Mediterranean atmosphere, J. Geophys. Res., 103, 13 137–13 144.

Navas-Guzman, F. Bravo-Aranda, J. A. Guerrero-Rascado, J. L. Granados-Munoz, M. J. Alados-Arboledas, L., 2013. Statistical analysis of aerosol optical properties retrieved by Raman lidar over Southeastern Spain. Tellus B. 65 21234.

Obregon, M. A. Pereira, S. Salgueiro, V. Costa, M. J. Silva, A. M. Serrano, A. Bortoli, D. 2015. Aerosol radiative effects during two desert dust events in August 2012 over the Southwestern Iberian Peninsula. Atmos.Res. 153. 404-415.

O'Neill, N. T., Dubovik, O., and Eck, T. F., 2001a. A modified Ångström coefficient for the characterization of sub-micron aerosols, Appl. Opt., 40, 2368–2375.

O'Neill, N. T., Eck, T. F., Holben, B. N., Smirnov, A., and Dubovick, O., 2001b. Bimodal size distribution influences on the variation of Ångström derivatives in spectral and optical depth space, J. Geophys. Res., 106(D9), 9787–9806,.

O'Neill, N. T., Eck, T. F., Smirnov, A., Holben, B. N., and Thulasiraman, S., 2003. Spectral discrimination of coarse and fine mode optical depth, J. Geophys. Res., 108(D17), 4559.

Papayannis, A., V. Amiridis, L. Mona, G. Tsaknakis, D. Balis, J. Bösenberg, A. Chaikovski, F. De Tomasi, I. Grigorov, I. Mattis, V. Mitev, D. Müller, S. Nickovic, C. Pérez, A. Pietruczuk, G. Pisani, F. Ravetta, V. Rizi, M. Sicard, T. Trickl, M. Wiegner, M. Gerding, R.E. Mamouri, G. D'Amico, and G. Pappalardo, 2008. Systematic lidar observations of Saharan dust over Europe in the frame of EARLINET (2000-2002). J. Geophys. Res., 113, D10204,

Pappalardo, G., Amodeo, A., Apituley, A., Comeron, A., Freudenthaler, V., Linné, H., Ansmann, A., Bösenberg, J., D'Amico, G., Mattis, I., Mona, L., Wandinger, U., Amiridis, V., Alados-Arboledas, L., Nicolae, D., and Wiegner, M., 2014. EARLINET: towards an advanced sustainable European aerosol lidar network, Atmos. Meas. Tech., 7, 2389-2409.

Pavese, G. Calvello, M. F. de Tomasi, Peroone, M. R. 2009. Detection of Sahara dust intrusions during mixed advection patterns over south-east Italy: A case study. 92 (4). 489-504.

Perez, C. Nickovic, S. Baldasano, J. M. Sicard, M. Rocadenbosch, F. and Cachorro, V. E. 2006. A long Saharan dust event over the western Mediterranean: Lidar, Sun photometer observations, and regional dust modeling, J. Geophys. Res., 111, D15214.

Perez-Ramirez, D., Lyamani, H., Olmo, F. J., Whiteman, D. N. and Alados-Arboledas, L. 2012. Columnar aerosol properties from sun-and-star photometry: statistical comparisons and day-to-night dynamic. Atmos. Chem. Phys. 12, 9719–9738.

Perrone, M. R. Bergamo, A. 2011. Direct radiative forcing during Sahara dust intrusions at a site in the Central Mediterranean: Anthropogenic particle contribution. 101 (3). 783-798.

Pey, J. Querol, X. Alastuey, A. Forastiere, F. and Stafoggia, M., 2013. African dust outbreaks over the Mediterranean Basin during 2001–2011: PM10 concentrations, phenomenology and trends, and its relation with synoptic and mesoscale meteorology, Atmos. Chem. Phys., 13, 1395–1410.

Piedeherro, A. A. Anton, M. Carzola, A. Alados-Arboledas, L. Olmo, F-. J. 2014. Evaluation of enhancement events of total solar irradiance during cloudy conditions at Granada (Southeastern Spain). Atmos. Res. 135-136. 1-7.

Prospero, J.M., Ginoux, P., Torres, O., Nicholson, S., Gill, E., 2002. Environmental characterization of global sources of atmospheric soil dust identified with the NIMBUS-7 total ozone mapping spectrometer (TOMS) absorbing aerosol product. Rev. Geophys. 40 (1), 1002.

Ramanathan, V. Ramana, M. Roberts, G. Kim, D. Corrigan, C. Chung, C. and Winker D., 2007. Warming trends in Asia amplified by brown cloud solar absorption, Nature, 448, 575– 578.

Sabbah, I., Ichoku, C., Kaufman, Y. J., and Remer, L., 2001. Full year cycle of desert dust spectral optical thickness and precipitable water vapor over Alexandria, Egypt, J. Geophys. Res., 106, 18305–18316.

Schuster, G. L., Dubovik, O., and Holben, B. N., 2006. Ångström exponent and bimodal aerosol size distributions, J. Geophys. Res, 111, D07207.

Sicard, M., Pérez, C., Rocadenbosch, F., Baldasano, J.M. , García-Vizcaino, D., 2006. Mixed-layer depth determination in the Barcelona coastal area from regular lidar measurements: methods, results, and limitations, Boundary-Layer Meteorol., 119, 135 – 157.

Sicard, M. Rocadenbosch, F. Reba, M. N. M. Comeron, A. Tomas, S. Garcıa-Vızcaino, D. Batet O. Barrios, R. Kumar, D. and Baldasano, J. M., 2011. Seasonal variability of aerosol optical properties observed by means of a Raman lidar at an EARLINET site over Northeastern Spain, Atmos. Chem. Phys., 12, 3115–30.

Sicard, M. D'Amico, G. Comerón, A. Mona, L. Alados-Arboledas, L. Amodeo, A. Baars, H. Belegante, L. Binietoglou, I. Bravo-Aranda, J. AFernández, A. J. Fréville, P. García-Vizcaíno, D. Giunta, A. Granados-Muñoz, M. J. Guerrero-Rascado, J. L. Hadjimitsis, D. Haefele, A. Hervo, M. Iarlori, M. Kokkalis, P. Lange, D. Mamouri, R. E. Mattis, I. Molero, F. Montoux, N. Muñoz, A. Muñoz Porcar, C. Navas-Guzmán, F. Nicolae, D. Nisantzi, A. Papagiannopoulos, N. Papayannis, A. Pereira, S. Preißler, J. Pujadas, M. Rizi, V. Rocadenbosch, F. Sellegri, K. Simeonov, V. Tsaknakis, G. Wagner, F. and Pappalardo, G. 2015. EARLINET: potential operationality of a research network, Atmos. Meas. Tech., 8, 4587-4613.

Smirnov, A., Holben, B. N., Kaufman, Y. J., Dubovik, O., Eck, T. F., Slutsker, I., Pietras, C., and Halthore, R., 2002. Optical properties of atmospheric aerosol in maritime environments, J. Atmos. Sci., 59, 501–523.

Sokolik, I. N. Winker, D. M. Bergametti, G. Gillette, D. A. Carmichael, G. Kaufman, Y. J. Gomes, L. Schuetz, L. and Penner J. E., 2001. Introduction to special section: Outstanding problems in quantifying the radiative impacts of mineral dust, J. Geophys. Res., 106(D16), 18015– 18027.

Tanre, D. Kaufman, Y. J. Holben, B. N. Chatenet, B. Karnieli, A. Lavenu, F. Blarel, L. Dubovik, O. Remer, L. A. and Smirnov, A., 2001. Climatology of dust aerosol size distribution and optical properties derived from remotely sensed data in the solar spectrum, J. Geophys. Res., 106, 18205–18217.

Tegen, I. Lacis, A. A. and Fung, I., 1996. The influence on climate forcing of mineral aerosols from disturbed soils, Nature, 380, 419– 422.

Valenzuela, A. Olmo, F. J. Lyamani, H. Antón, M. Quirantes, A. Alados-Arboledas, L., 2012. Classification of aerosol radiative properties during African desert dust intrusions over southeastern Spain by sector origins and cluster analysis. J. Geophys. Res., 117, D06214.

Figure

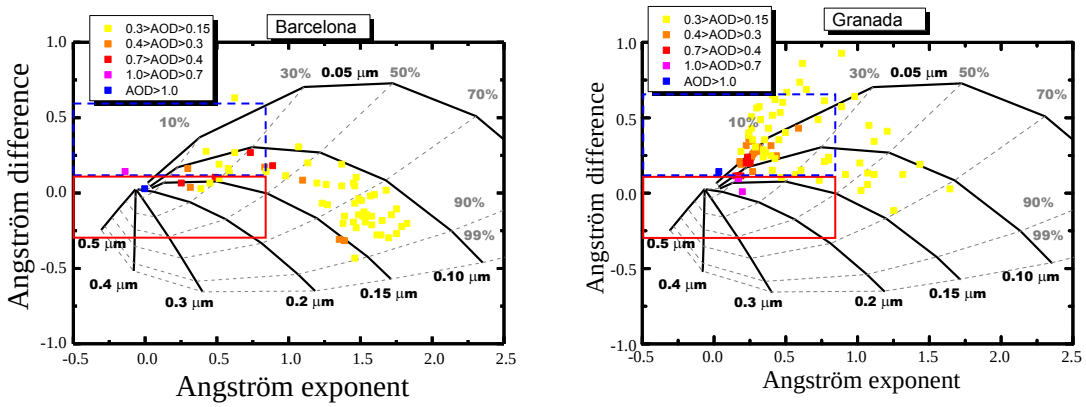

Fig 1. Ångström exponent difference $\delta\alpha=AE_{440\text{-}675}-AE_{675\text{-}870}$, as a function of the 440-870 nm Ångström exponent and AOD_{675} for two AERONET stations; Barcelona and Granada, during the investigated period. The solid lines are each for a fixed size of the fine mode R_f and the dashed lines for a fixed fraction contribution η of the fine mode to the AOT at 675 nm. The solid red box correspond to the days with coarse mode domination ($AOD_{675}>0.15$, $AE_{440\text{-}870}<0.75$ and $-0.3<\delta\alpha<0.1$), which are of the interest. Meanwhile the dashed blue box correspond to the days with the bimodal pattern ($AOD_{675}>0.15$, $AE_{440\text{-}870}<0.75$ and $0.1<\delta\alpha<0.6$).

Figure

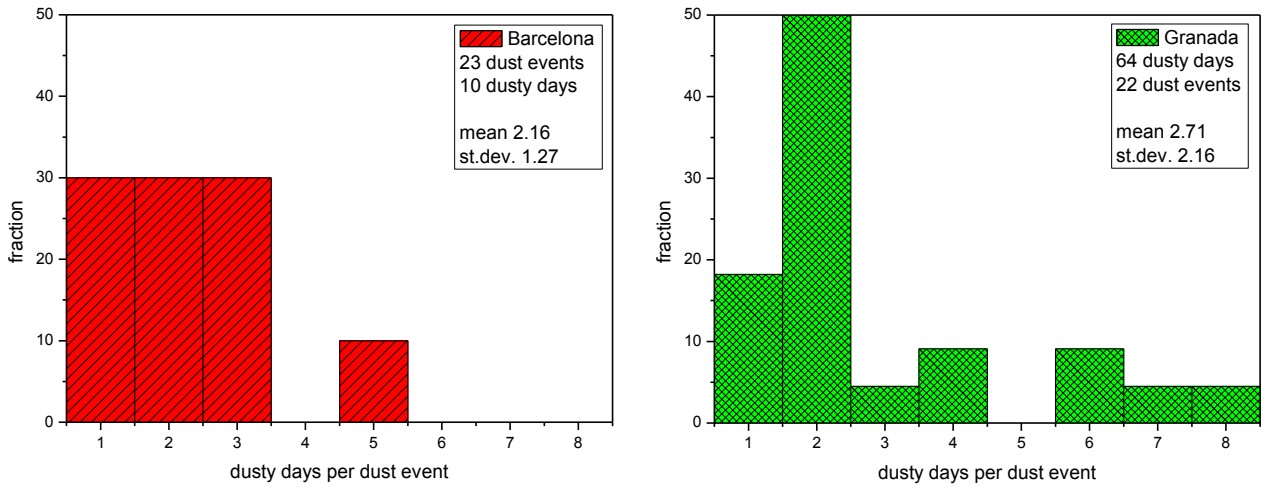

Fig 2. The distributions of the numbers of dusty days per each dust event; Barcelona and Granada

Figure

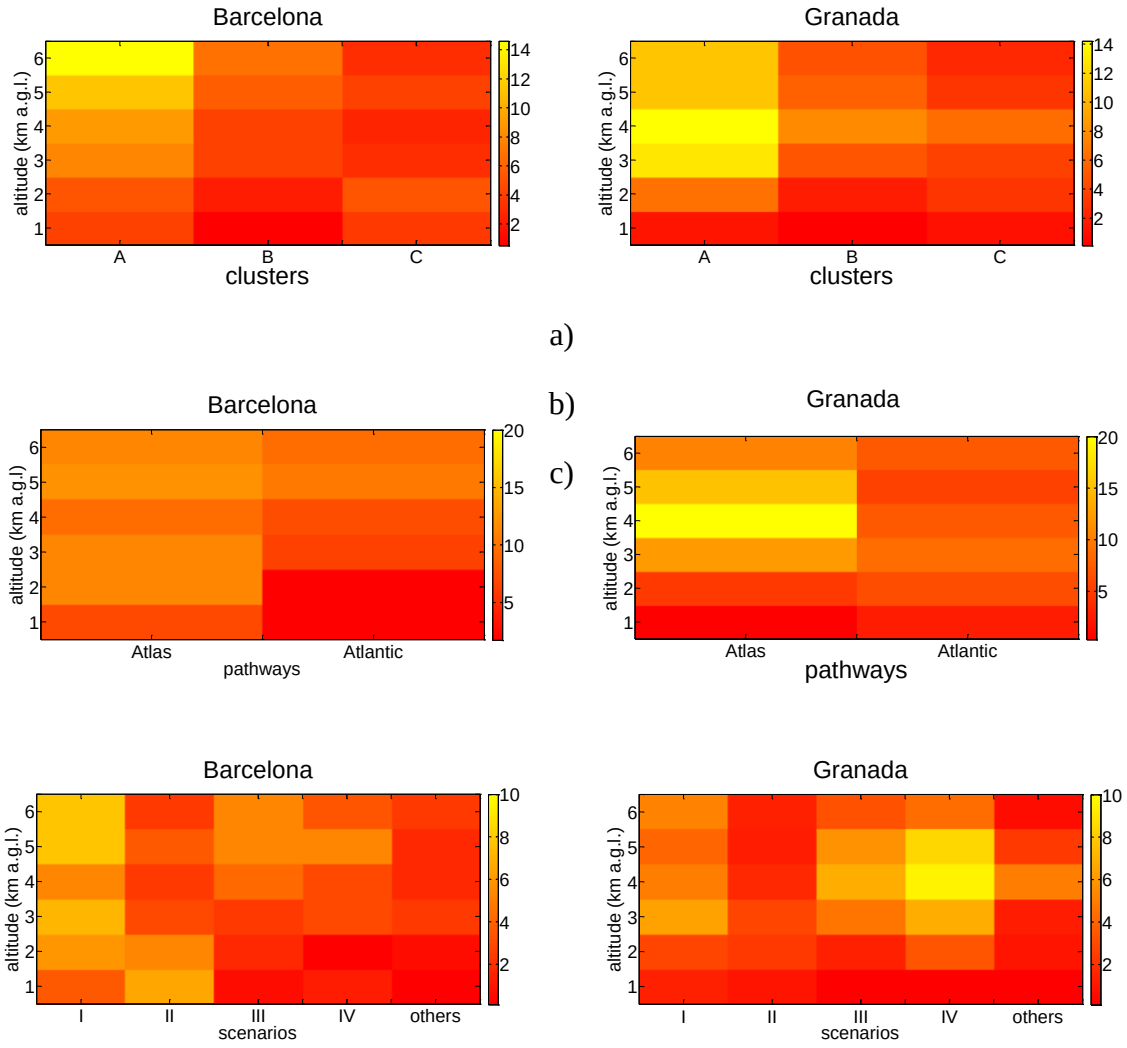

Fig 3. Percentage of back-trajectories at each altitude range (km a.g.l.)

a) according to their origins; A, B and C. Cluster A lays over the Morocco and west of Algeria, cluster B lays over West Sahara, Mauritania, south of Algeria and north of Mali, and cluster C lays over the remaining part of Algeria and Tunisia.

b) according to their pathways; overpppassing Atlas Mountains and with Atlantic arch pathway.

c) according to the dust intrusion scenarios; scenario I (cluster A with pathways through the Atlas Mountains), scenario II (cluster C with pathways through the Atlas Mountains), scenario III (cluster B with Atlantic arch pathway), scenario IV (cluster A with Atlantic arch pathway) and scenario V (the remaining scenarios).

Figure

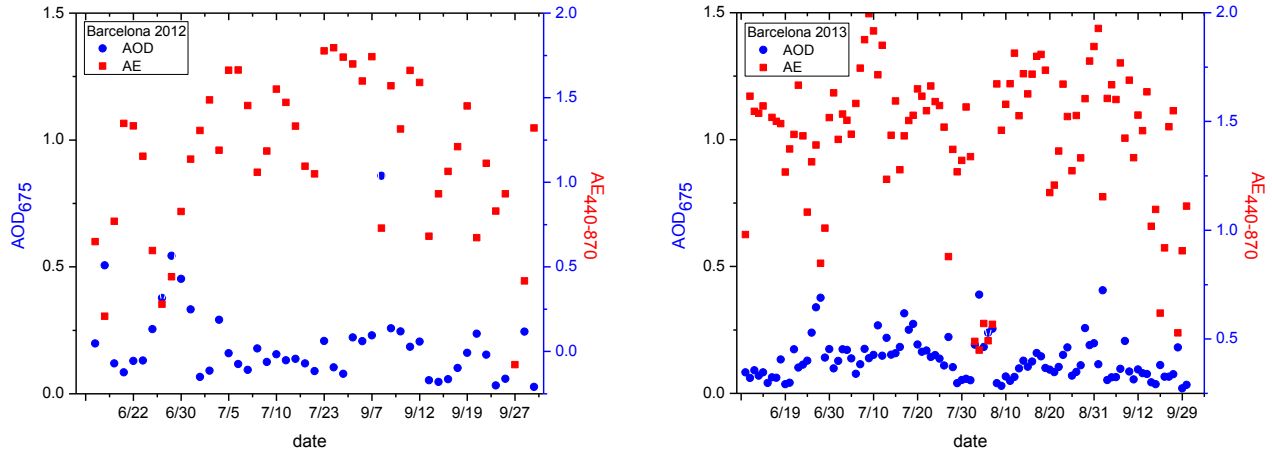

a)

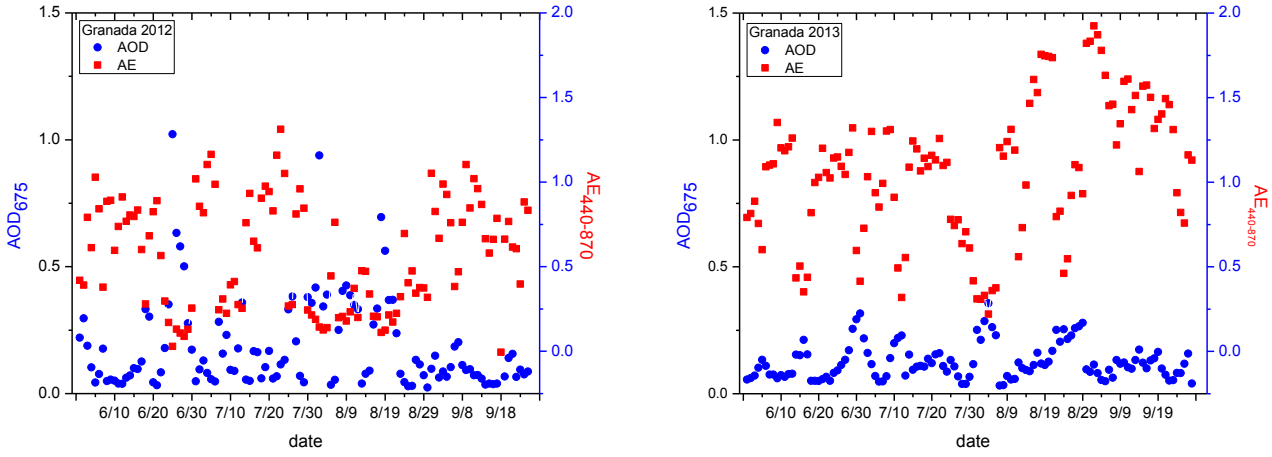

b)

Fig 4. Time-plots of AOD_{675} and $AE_{440\text{-}870}$ during the whole period June –September 2012 and 2013

a) in Barcelona (2012, 2013)
b) in Granada (2012, 2013)

Figure

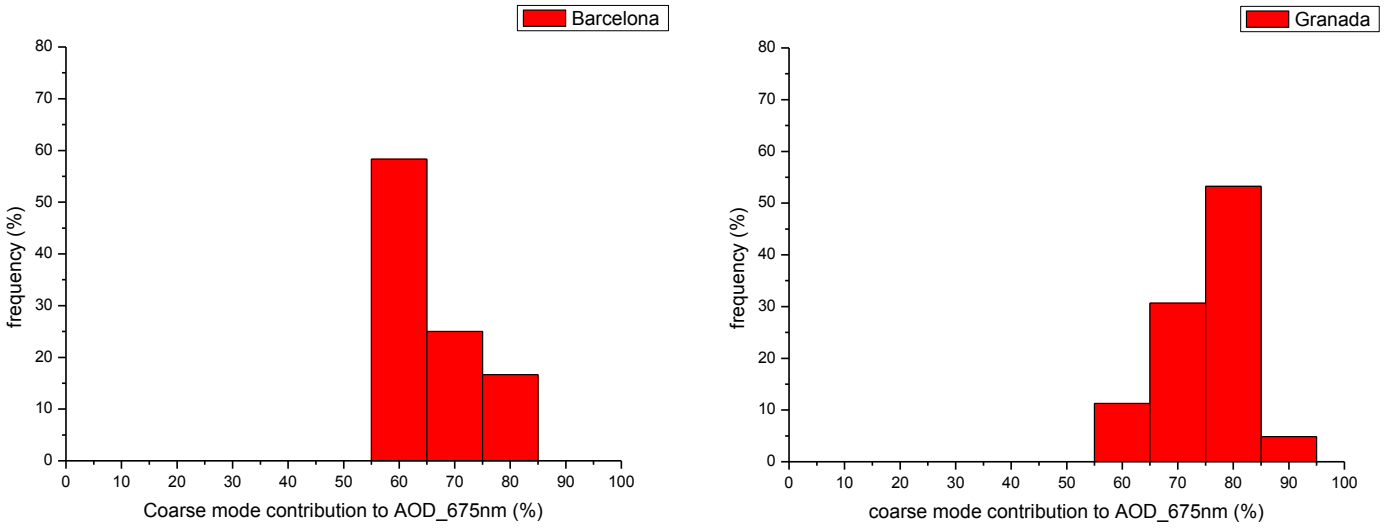

Fig 5. Statistical distributions of coarse mode contribution on AOD_{675} during dusty days in Barcelona and Granada. The most frequent coarse mode contribution on AOD was found 60% at Barcelona and 80% at Granada station.

Figure

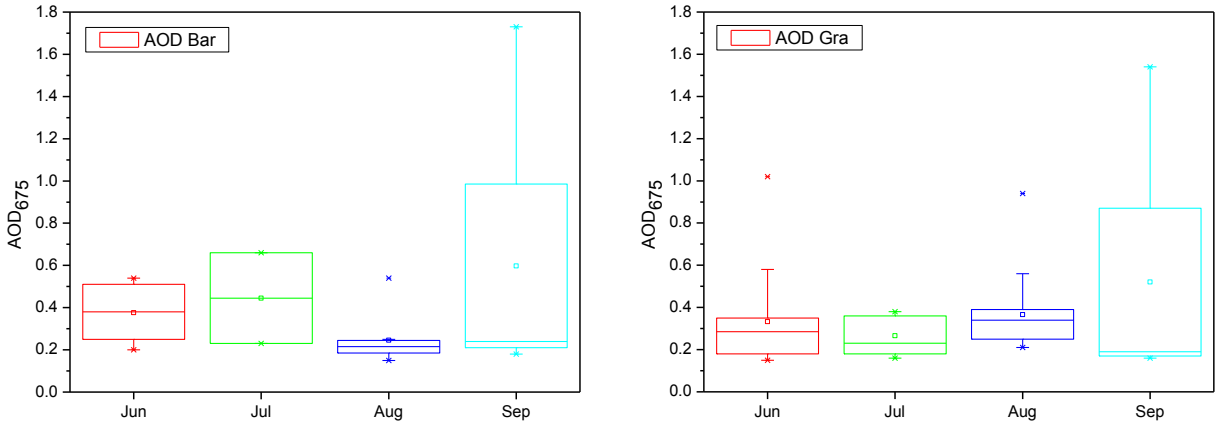

a)

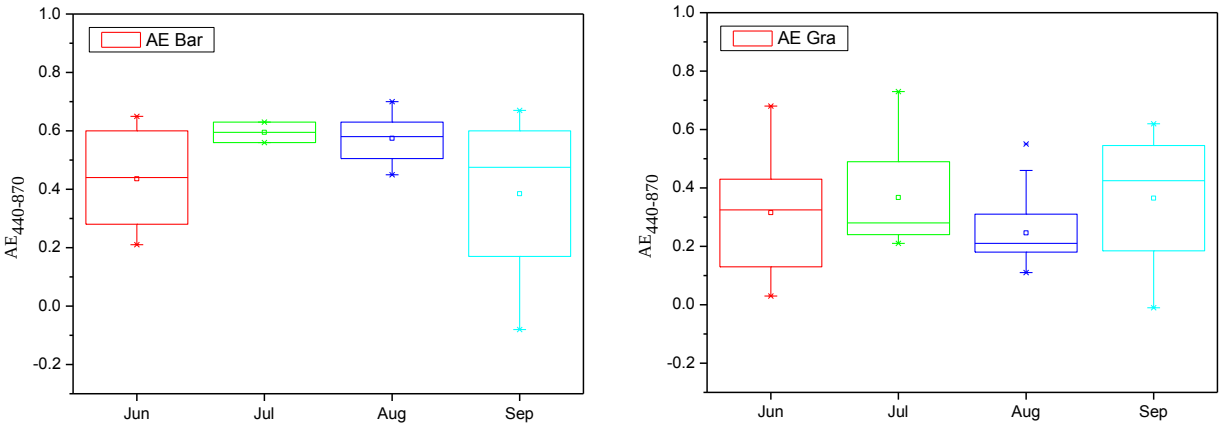

b)

Figure 6. Statistical distribution of the aerosol optical properties in Barcelona and Granada during dusty days of each month. Median, minimal, maximal, first and third quartiles of the AOD and AE values are presented in these plots.

a) Aerosol optical depth AOD_{675}
b) Angstrom exponent $AE_{440\text{-}870}$

Figure

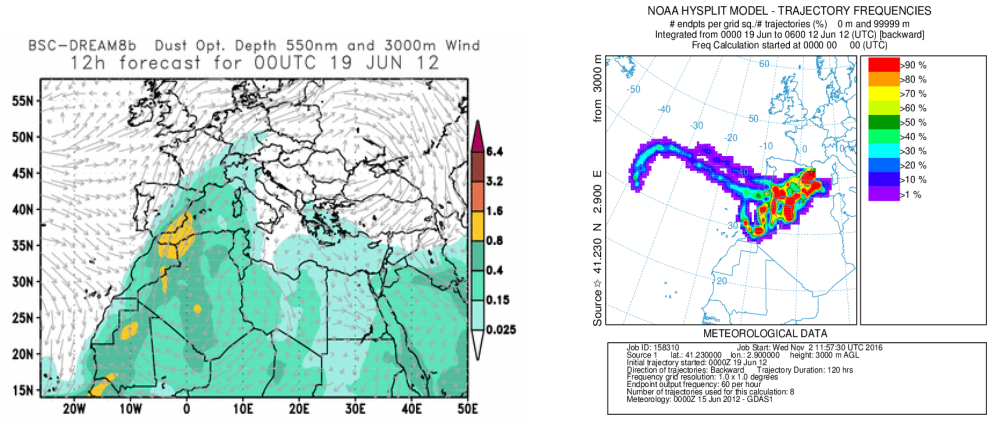

a)

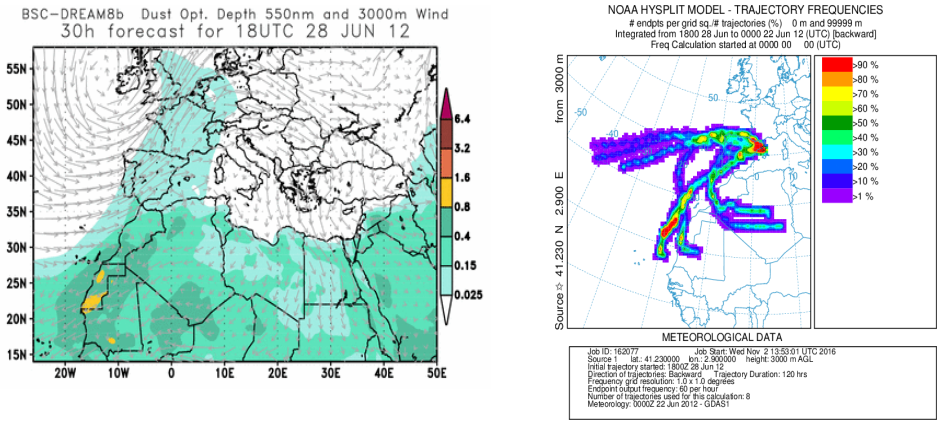

b)

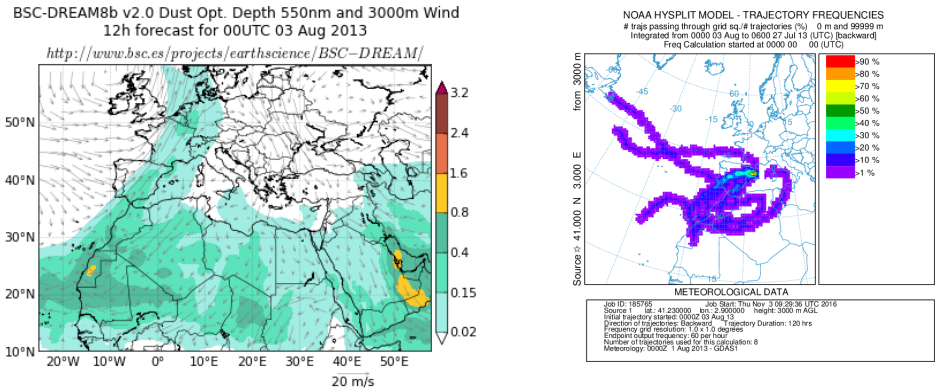

c)

Figure 7. Maps provided by the models DREAM (on the left) and HYSPLIT (on the right) for three coincidence dust events under analysis. a) Dust Event I, b) Dust Event II and c) Dust Event III. According to these maps, Dust Event I follows the scenario III, Dust Event II follows scenarios III and IV, and Dust Event III follows the scenario III.

Figure

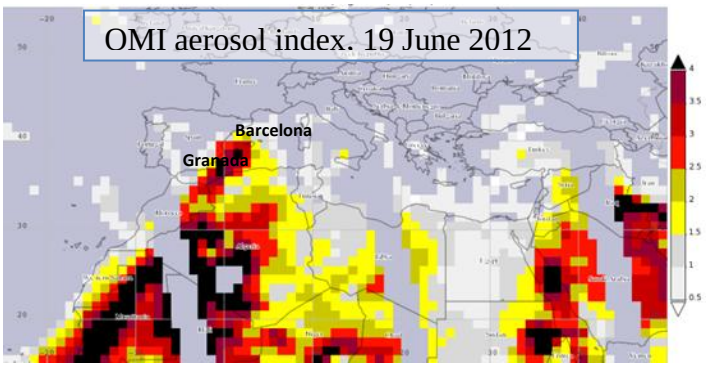

(a)

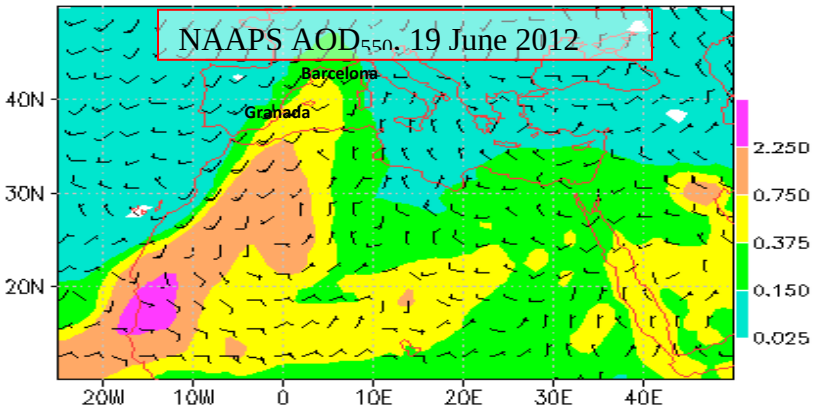

(b)

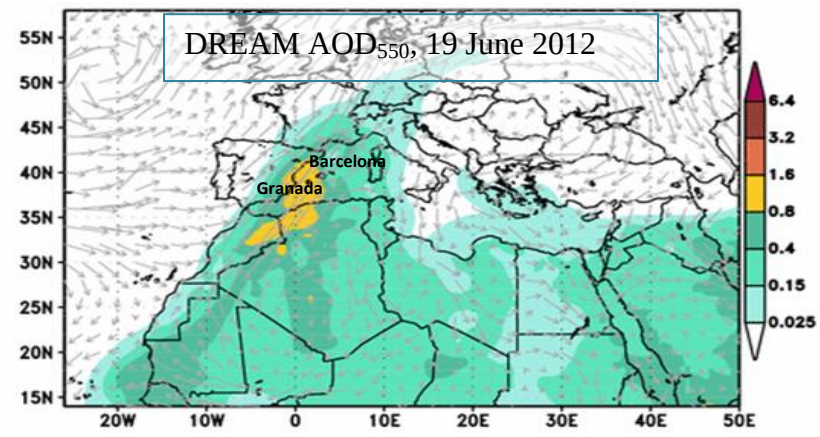

(c)

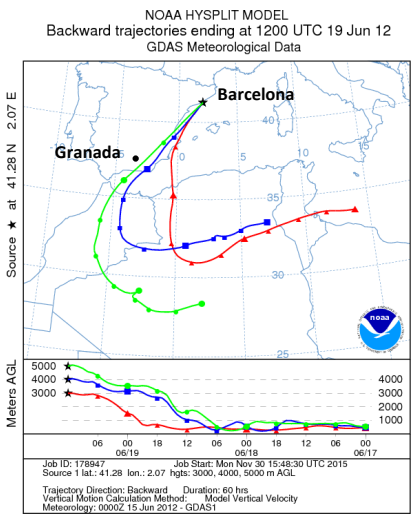

(d)

Fig 8. Some of the tools used to classify event I (18-19 June 2012) as a coincident dust event: daily OMI aerosol index on 19 June; NAAPS and DREAM maps of dust AOD at 550 nm on 19 June at 12 UT; Hysplit back trajectories arriving in Barcelona on 19 June at 12 UT.

Figure

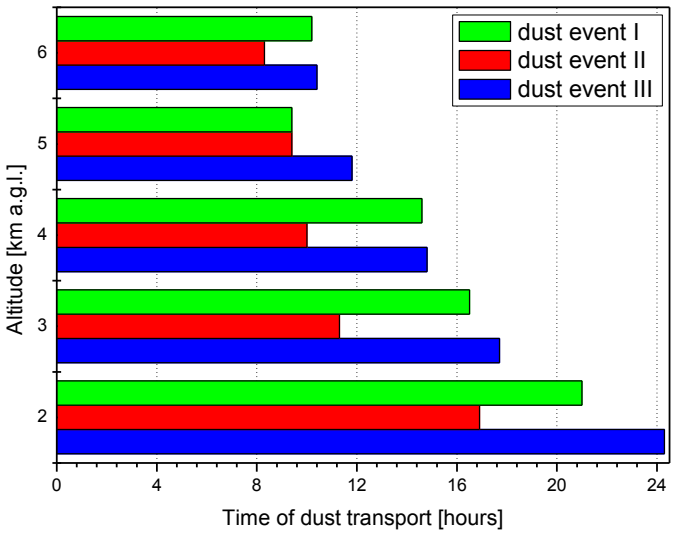

Fig 9. Temporal mean time of the dust plume transport from Granada to Barcelona as a function of height during the three coincident dust events.

Figure

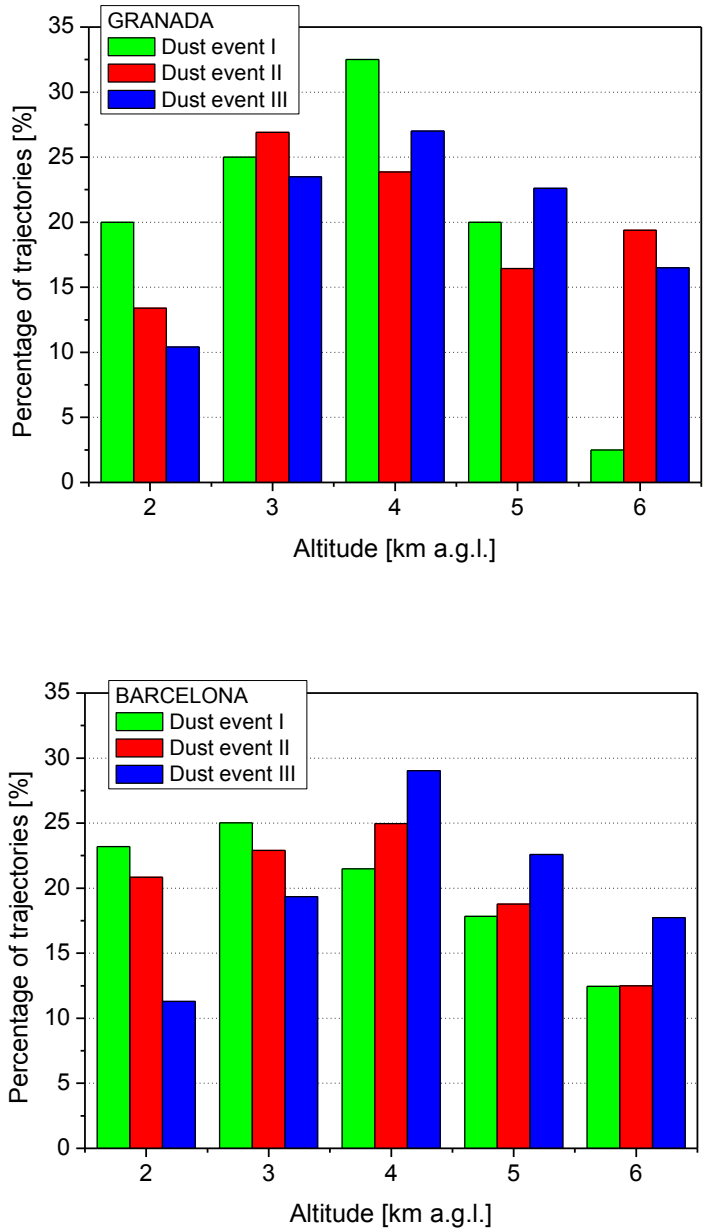

Fig 10. Normalized numbers of the back-trajectories by height originating in the Saharan region and overpassing Granada and Barcelona during the three dust events.

Figure

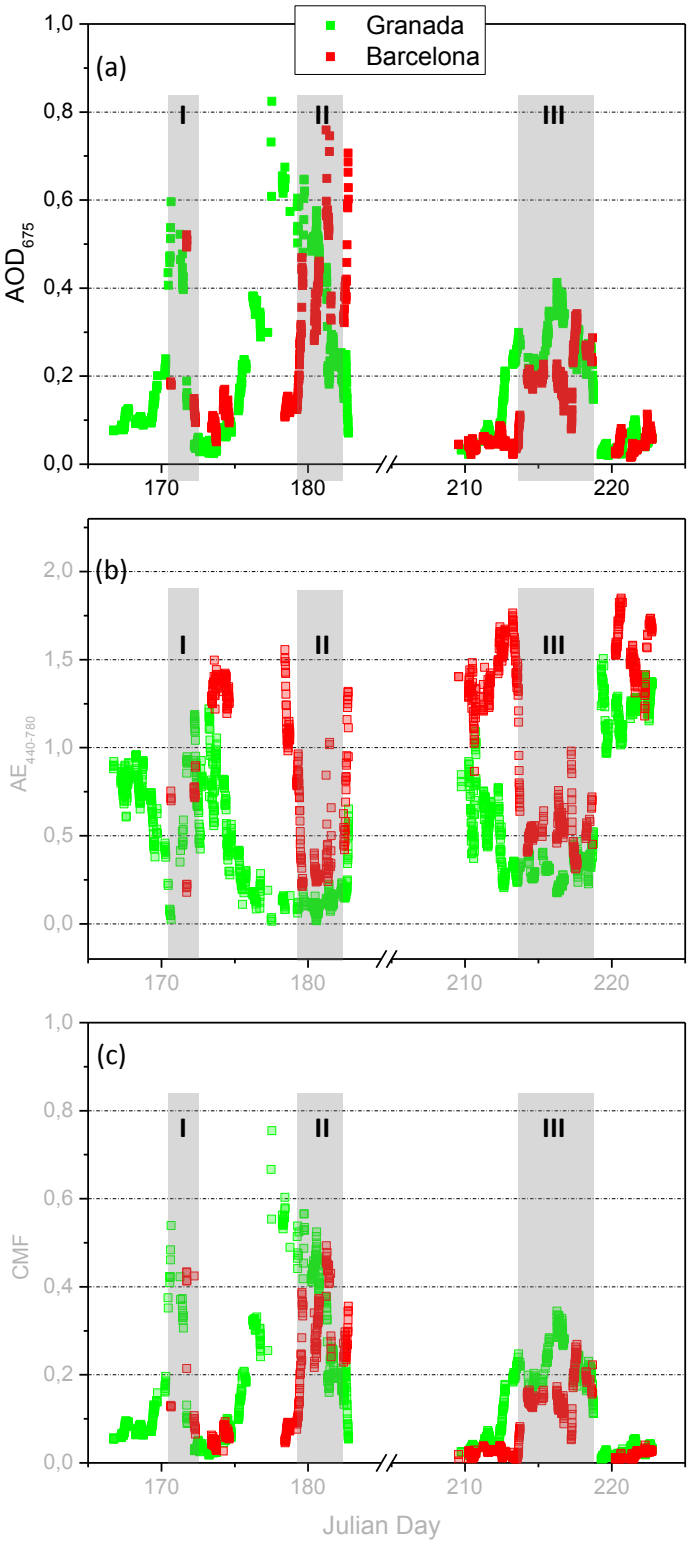

Fig 11. Temporal variation of (a) AOD at 675 nm, (b) Ångström exponent calculated between 440 and 870 nm and (c) the coarse mode fraction, at Granada and Barcelona. The gray bars indicate the coincident periods considered for the comparison between both sites.

Figure

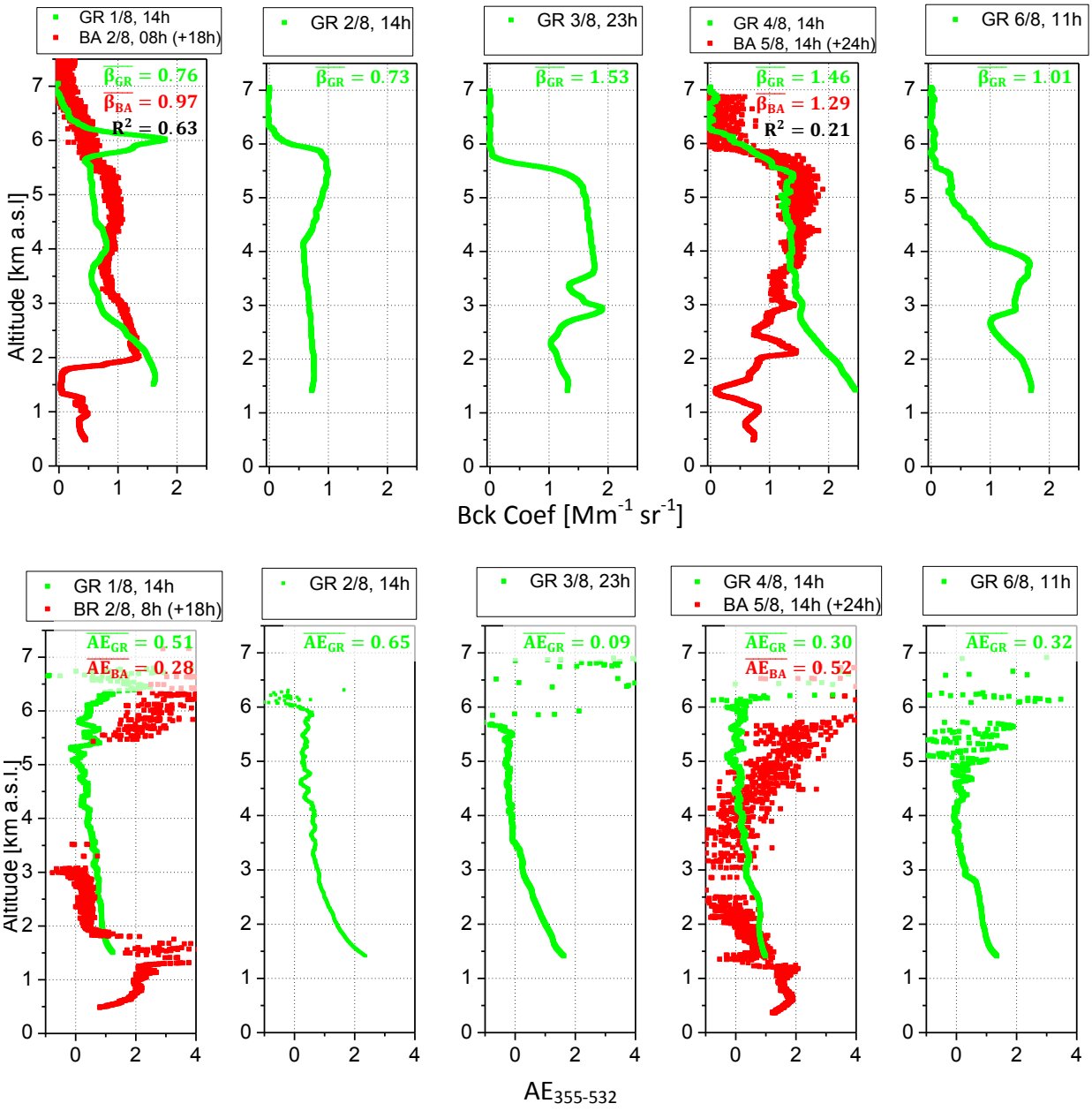

Fig 12. 30-min. averaged profiles of the (top) backscatter coefficient at 532 nm and of the (bottom) backscatter Ångström exponent calculated with the wavelengths at 355 and 532 nm during dust event III (1 - 6 August 2013). GR and BA stand for Granada and Barcelona, respectively. No data are available in Granada on 5 August and in Barcelona on 3 and 4 August. $\overline{\beta}$ and $\overline{AE}$ represent respectively the average backscatter coefficient (given in Mm^{-1}·sr^{-1}) and backscatter Ångström exponent in the 2 – 5.5 km range. R^2 is the correlation coefficient between the Granada and Barcelona profiles calculated in the range 2 – 5.5 km.

Table

Table 1. Number of dusty days and dust events in Barcelona and Granada AERONET sites.

	Dusty days				
	June Total/12/13	July Total/12/13	August Total/12/13	September Total/12/13	Total Total/12/13
Barcelona	5/5/0	2/2/0	12/7/5	4/3/1	23/17/6
Granada	18/13/5	15/11/4	25/17/8	6/6/0	64/47/17
	Dust events				
Barcelona	2/2/0	1/1/0	4/3/1	3/2/1	10/8/2
Granada	6/4/2	7/5/2	5/3/2	4/4/0	22/16/6

Table

Table 2. Cluster analysis of air masses; cluster sources and the pathways during the dust events over Barcelona and Granada

Clusters		
Category	Barcelona	Granada
Cluster A	61.0%	53.0%
Cluster B	20.9%	35.4%
Cluster C	18.1%	11.6%
Pathways		
Atlas	62.4%	54.1%
Atlantic	37.6%	45.9%

Table

Table 3. Mean AOD_{675} and $AE_{440\text{-}780}$ (and standard deviation) during different scenarios in Barcelona and Granada

	Barcelona				Granada			
	Scen. I	Scen. II	Scen. III	Scen. IV	Scen. I	Scen. II	Scen. III	Scen. IV
AOD	0.30±0.14	0.35±0.18	0.24±0.08	0.25±0.07	0.36±0.20	0.46±0.32	0.36±0.26	0.31±0.200
AE	0.53±0.13	0.54±0.13	0.53±0.06	0.58±0.09	0.28±0.13	0.25±0.13	0.24±0.14	0.31±0.15
h (km)	3.7	3.5	5.0	4.2	4.1	3.6	4.1	4.2
Freq.(%)	46.5	21.2	14.8	17.4	39.7	11.2	33.9	15.2

Table

Table 4. Temporal mean AOD at 675 nm, AOD_{675}, Ångström exponent calculated between 440 and 870 nm, $AE_{440\text{-}870}$, and coarse mode fraction, *CMF*, for each dust event in Granada and in Barcelona.

	Dust event I			Dust event II			Dust event III		
	18-19 June 2012 (2 days)			27-29 June 2012 (3 days)			2-6 August 2013 (5 days)		
	Scenario I			Scenario III and IV			Scenario III		
Parameter	AOD_{675}	$AE_{440\text{-}870}$	CMF	AOD_{675}	$AE_{440\text{-}870}$	CMF	AOD_{675}	$AE_{440\text{-}870}$	CMF
Granada	0.39	0.35	0.74	0.43	0.11	0.84	0.28	0.30	0.74
Barcelona	0.28	0.51	0.65	0.42	0.45	0.66	0.23	0.53	0.63
Difference (Bar. – Gra.)	-0.11	+0.16	-0.09	-0.01	+0.34	-0.18	-0.05	+0.23	-0.11